A rising trend of double tropopauses over South Asia in a warming environment: implications for moistening of the lower stratosphere

Suvarna Fadnavis[1*], Christopher E. Sioris[2], Neeraj Wagh[3], Rajib Chattopadhyay[1], Mengchu Tao[4], Prashant Chavan[1] and Tanusri Chakroborty[1]

[1]Indian Institute of Tropical Meteorology, Ministry of Earth Sciences, India

[2]Atmospheric Science and Technology Directorate, Environment and Climate Change Canada, Toronto, Canada

[3]University of Illinois Urbana-Champaign, Department of Statistics, United States of America

[4]Forschungszentrum Jülich (IEK-7: Stratosphere), Jülich, Germany

*Corresponding author email:suvarna@tropmet.res.in

Abstract

The water vapor variation in the upper troposphere and lower stratosphere (UTLS) is of high significance due to its impact on global warming. In this paper, we present an association of occurrence frequency of double tropopauses (DTs) with convective clouds and transport of water vapor in the UTLS over subtropical South Asia using multiple multi-decadal datasets (e.g., radiosonde temperature profiles (1977 – 2017), Atmospheric Infrared Sounder (2003 – 2017), ERA-Interim reanalysis (1979 – 2017), and Microwave Limb Sounder (2004 – 2016). The diagnostic analysis of temperature, water vapor, and potential vorticity indicates that convective clouds occurring during DTs enhance water in the altitude layer near the DTs. DTs are frequent (~5 – 55 %) over the subtropical South Asia (25° – 30°N) and associated with an enhancement of water vapor mixing ratios by ~5 – 40 % (0.2 – 7.5 ppmv) above the lower tropopause.

The radiosonde observations show a positive trend (~0.27 ± 0.12 to 0.4±0.2 %/year) in the occurrence of DTs during last 45 years, enhancing the moisture during DT days (trend 0.04±0.02 to 0.26±0.24 ppmv/decade above the tropopause). The convective injection of anomalously high water vapour mixing ratios in DT conditions and moistening trends in the UTLS may be consequences of global warming. The increasing trend in the water vapor in the UTLS may enhance long-wave radiation coming back down to warm the troposphere and exacerbate the global warming effect.

Keywords: Wyoming radiosonde temperature; Upper Troposphere and Lower Stratosphere (UTLS); Double tropopause; ERA-Interim water vapor and temperature.

1. Introduction

The variation of water vapor near the tropical tropopause has a significant impact on climate change via radiative forcing (Solomon *et al.*, 2010). Water vapor increases in the upper troposphere due to convection contribute nearly a fifth of the atmospheric radiative heating anomaly (Harrop and Hartmann 2015). The Asian summer monsoon plays a vital role in transporting water vapor into the upper troposphere and lower stratosphere (Gettelman *et al.*, 2004). Other than monsoon convection, the South Asian region frequently experiences the occurrence of convective systems (e.g., cyclones, thunderstorms, etc.) due to the presence of conditional instability. Convective systems inject water vapor into the atmosphere, and the pre-moistened environment favors the development of convection (Virts and Houze, 2015). The clouds associated with convective systems usually reach near the tropopause over South Asia (Jensen and Del Genio, 2003). Such cloud tops favor stratosphere-troposphere exchange (STE), causing significant variations of water vapor and temperature via mixing of moist/dry and warmer/colder air in the upper troposphere and lower stratosphere (UTLS) (Sausen and Santer, 2003; Riese *et al*., 2012; Randel and Jensen, 2013; Fadnavis and Chattopadhyay, 2017).

Various observations, e.g., aircraft, radiosonde, GPS radio occultation, and satellites show that double tropopause (DT) events in the mid-latitudes are associated with water vapor enhancements in the UTLS (Homeyer et al., 2014). Simultaneous radar and aircraft observations at mid-latitudes reveal that deep overshooting at altitudes up to 4 km above the lapse-rate tropopause are co-located with enhanced water vapor ~60 – 225 ppmv (background 5 – 10 ppmv) at altitudes 1-2 km above the tropopause (Homeyer *et al.*, 2014). In the presence of a double tropopause, overshooting is deeper and increases as the stability of the lower stratosphere decreases (Solomon *et al*, 2016). The

gravity waves generated from convection propagate into the lower stratosphere. The wave breakdown induces irreversible mixing and amplifies the vertical transport of water vapor (Lane and Sharman, 2006) .

The National Center for Atmospheric Research Community Atmosphere Model simulations show that the frequency of tropopause-overshooting deep convective clouds (DCCs) increases by 21 % per 1 K warming of the tropical oceans (Aumann *et al*., 2018). The future projections from the Coupled Model Inter-comparison Project show a 2.7 K increase in the surface temperature of the tropical oceans by the end of this century. The warming of the oceans may increase the frequency of DCC in the tropics by about 60 % (Aumann *et al.*, 2018). Thus, in the future, convective transport of water vapor into the lower stratosphere may amplify the positive feedback of global warming. The global warming feedback of water vapor is comparable to the warming by CO_2 (Dessler *et al.*, 2013; Ingram, 2010).

Over South Asia, surface temperatures are rising since the past 70 years (1951 to 2013) (Ross *et al.*, 2018). The consequences of this warming are observable in many ways, e.g. (1) Indian Ocean warming of 1.2 K during 1901 – 2012 (Roxy *et al.* 2014), (2) a rising trends in frequency of occurrence of DCCs ~ +1.05 ± 0.29 % yr^{-1} over the Indian Ocean and +3.15 ± 0.030 % yr^{-1} over the Indian lands, evident in Atmospheric Infrared Sounder (AIRS) data during 2002 – 2012 (Aumann and Ruzmaikin, 2013), (3) the strengthening of the equator-ward temperature gradient and consequently enhanced baroclinic wave activity in the UTLS over the subtropics. An increase of wave baroclinicity increases the frequency of occurrences of DTs. DTs are increasing in a warming environment (Castanheira *et al*. 2009). The association of DTs with deep convection and

water vapor transport into the UTLS is not fully explored over the warming South Asian region. It is important to understand their association, if any, since injected anomalously high water vapor (during DT events) is further transported deep into the stratosphere via the Brewer–Dobson circulation (BDC) and quasi-horizontally into the extratropical lower stratosphere (Rolf *et al.*, 2018).

The formation of double tropopauses (DTs) in the UTLS is one of the processes associated with stratosphere-troposphere exchange (STE) (Pan *et al.*, 2009; Peevey *et al.*, 2014). Previous studies show that STE processes (associated with Rossby wave breaking) produce considerable variability of water vapor in the UTLS (Ploeger *et al.*, 2013; Homeyer *et al.*, 2014). On a large scale, DTs can be indicative of poleward Rossby wave breaking that carries subtropical upper tropospheric moist air into the extra-tropical lower stratosphere (Ploeger *et al.*, 2013). DTs are ubiquitous over mid-latitudes (DT occurrence frequency 50 – 70 %) in boreal winter in the northern hemisphere and their frequency is lower in the tropics (Randel *et al.*, 2007; Peevey et al., 2012). The thickness of the double tropopause layer (i.e., altitude difference between first and second tropopause) varies with latitude. High-Resolution Dynamics Limb Sounder data show an increase in the thickness of this layer with latitude (Peevey *et al.*, 2012). The existing literature indicates that there are different mechanisms for the formation of DTs in mid-latitudes. Some of the studies state that, in mid-latitudes, the higher tropical tropopause overlaps with, the lower polar tropopause, forming a characteristic break in the thermal tropopause along the subtropical jet, which results in the formation of the double tropopauses (DTs) (Pan *et al*., 2009; Peevey *et al.*, 2012). Poleward Rossby wave breaking transports low latitude air masses to the extra-tropics, leading to double tropopause conditions (Randel *et al.*, 2007; Pan *et al*., 2009; Peevey *et al.*, 2012; Homeyer *et al.*, 2014). Wang and Polvani (2011) illustrate that the air mass between the two

tropopauses can originate from high latitudes. They report that DTs arise due to an evolution of mid-latitudes baroclinic eddies if the extra-tropical tropopause inversion layer (TIL) is present initially. The strength of the TIL modulates the frequency of DT occurrences (Peevey et al., 2014). The TIL is a persistent feature while DTs are infrequent over the tropics. The DT structure in the tropics is quite complex due to its association with convection. A few studies pointed out that, on smaller scales, convection is an important moistener of the UTLS, and DTs enable deeper overshooting of the primary tropopause than single tropopause (ST) days (e.g., Homeyer et al., 2014; Solomon et al. 2016). However, the mechanisms for the formation of DTs are not completely understood (Wang and Polvani, 2011).

Observed evidence of the association of DTs with water vapor variability in the UTLS in the mid-latitude motivate us to explore characteristic features of DTs and associated water vapor variations over the highly polluted and convectively unstable south Asian region. The study has its focus on South Asia instead of the entire northern sub-tropical region because (1) DTs, and convection are frequent in the former, (2) because more frequent water vapor extremes are expected, (Homeyer *et al.*, 2014; Peevey *et al.* 2014) and (3) convective processes in South Asia show regional and seasonal variability (Manoharet al., 1999). The studies pertaining to details of the characteristic features of DTs over the South Asian region are sparse. The study region, South Asia, is the source of large emissions of greenhouse gases and aerosols (Fadnavis *et al.*, 2013; 2014; Fadnavis and Chattopadhyay, 2017; Roy *et al.*, 2017). This convectively active region is known for uplifting greenhouse gases, aerosols and water to the UTLS, which influences the thermal structure of the tropical UTLS by altering the radiative forcing (Fadnavis *et al.*, 2013; 2014; Roy et al., 2017). Injection of pollutants and water vapor may amplify the water vapor feedback, leading to increased radiative forcing.

From satellite remote sensing data, we also provide of the association of DTs with convective clouds, since convection is instrumental in transporting water vapor to the UTLS. Further, we examine the trend in the occurrences of DTs and the trend in water vapor (for DT days) in the lower stratosphere over subtropical South Asia. Understanding these trends is important since it has been shown that a rising trend in water vapor in the UTLS has implications for climate change (Dessler et al., 2013).

2. Data and Analysis

2.1 Radiosonde observations

The upper air radiosonde observations of temperature provided by WMO are available at the University of Wyoming (http://weather.uwyo.edu/upperair/sounding.html) dating back to 1973. Measurements are performed twice daily (00:00 UTC and 12:00 UTC) and have a vertical resolution of ~30 m. The data has been archived at two stations over the subtropical South Asia (1) Gauhati (26.10° N, 91.58° E), and (2) Delhi (28.70° N, 77.10° E) (Figure 1a). These stations are spread over the northern part of South Asia (Delhi), and the north-east part of South Asia (Gauhati). In this study, we have analyzed radiosonde profiles available for the period January 1984 – December 2017 at Gauhati and January 1977 – December 2017 at Delhi. To check that Gauhati is within the monsoon anticyclone throughout the monsoon season, we plot the montgomery potential stream function at 350 K potential surface. Our analysis shows that it is situated within the anticyclone throughout the monsoon season for all the years (e.g. Fig S1 for August 2016).

The error estimates associated with the radiosonde temperature data are documented at https://www.weather.gov/upperair/Study2, and https://www.nws.noaa.gov/directives/sym/pd01014001curr.pdf. The minimum temperature difference between radiosonde measurements located at the center of a satellite radiometer scan spot of radius 55 km are < 1ºC for levels in the troposphere and lower stratosphere (Kitchen, 1989). We apply the World Meteorological Organization's (WMO's) Commission for Aerology criteria for DTs (WMO, 1957) on the radiosonde temperature profiles (1977 – 2017) to identify the occurrence of the DTs. "(a) The first tropopause is defined as the lowest level at which the lapse rate decreases to 2 ºC km^{-1} or less, provided also the average lapse rate between this level and all higher levels within 2 km does not exceed 2ºC km^{-1}. (b) If above the first tropopause the average lapse rate between any level and all higher levels within 1 km exceeds 3 °C km^{-1}, then a second tropopause is defined by the same criterion as under (a). This tropopause may be either within or above the 1 km layer". The individual sounding profiles are used to determine the location of the first lapse-rate tropopause (TR1) and, if present, the second tropopause (TR2). We have considered a profile valid for analysis if it extends to 27 km. Also, a profile is considered as invalid if the first tropopause is identified below 7 km and if tropopauses are not apart by 1 km. These filters eliminated ~11.7% of all profiles during 1977 - 2017. Figure 1a and 1b show two examples of radiosonde and ERA-Interim temperature profiles when DTs are identified. The vertical variation of temperature obtained by radiosonde and ERA-Interim on 18 January 2013 at Gauhati shows TR1 at 16.2 km and TR2 at 18.8 km, at Delhi, on 3 December 2017 (Fig. 1b), TR1 is at 11.2 km and TR2 at 16.8 km (Fig. 1c). Similarly, days with DTs are counted for computation of the frequency of occurrence of DTs. Also, altitudes and temperatures corresponding to TR1 and TR2 are compiled, and their monthly means (1977 – 2017) are analyzed at these stations. Fig1 b-c shows that DTs in ERA-Interim agrees with radiosonde (also see Fig. S2). Although altitudes of DTs in radiosonde and ERA-interim agree, the temperatures of the two tropopauses show biases

varying between 0 and 16 ºC. Tropopuase temperature and height of DTs identified in a radiosonde profile at 00 UTC and 12 UTC are averaged for a day since DTs persists for 3-8 days (discussed in section 3.3). Homeyer *et al.*, (2010), and Manney et al. (2017) report that DTs differ amongst the reanalyses due to differences in model grid and resolution. Therefore, the DTs identified from the radiosonde profiles are used for analysis of ERA-Interim reanalysis and MLS satellite observations as vertical resolution is prioritized. The ERA-Interim and MLS vertical resolutions are given in Section 2.2.

A long-term trend in occurrences of DTs is estimated from radiosonde profiles. Radiosonde profiles are available twice a day at 00 UTC and 12 UTC and therefore, in a month, one can expect 60 observations. However, the number of available observations varies at every station due to missing data. We consider a month valid for trend analysis only if the number of available observations in that month are > 30. There are 8 invalid months at Gauhati and 6 at Delhi during 1980-2017. The occurrence frequency of DT days for a month is relative number of DTs days / total available days). A trend value and standard deviation are estimated from time series of occurrences of DT days by using a least-squares fit method.

2.2 Satellite observations and reanalysis data

2.2.1 Atmospheric Infrared Sounder (AIRS)

The Atmospheric Infrared Sounder (AIRS) onboard the EOS (Earth Observing System) Aqua satellite provides information about atmospheric cloud properties, e.g., cloud top pressure (CTP, in hPa) and cloud top temperature (CTT, in K). The version 6 level 2 data are available

from 2003 to the present (https://airsl2.gesdisc.eosdisc.nasa.gov/data/Aqua_AIRS_Level2/AIRX2RET.006/) (Aumann *et al*.,2003;Kahn *et al*., 2014). The AIRS instrument measures radiances in 2378 spectral channels within a spectral range of 650- 2675 cm^{-1}. The spectral coverage includes strong CO_2 absorption bands necessary for temperature profile retrievals, window regions that are used for retrieving the surface and cloud properties, and a strong water vapor absorption band for humidity soundings. The maximum off-nadir scanning angle of AIRS is 49.5°, the swath width is 1650 km, and the footprint size is 13.5 km at nadir. With a 1:30/13:30 equator crossing time, AIRS orbit misses the peak in land-based convection (e.g., Aumann *et al.*, 2003). The cloud top altitudes obtained from AIRS and MODIS radiances show general agreement (Weisz *et al*., 2007). The convective clouds are classified into three categories (1) very deep convective clouds (VDCC); CTT < 220 K), (2) deep convective clouds (DCC; CTT = 220 – 235 K), and (3) convective clouds (CC; CTT = 235 – 255 K) when CTP < 400 hPa (Roca and Ramanathan, 2000). We extract the daily AIRS (level-2) cloud information within a 20 km periphery of the radiosonde stations during 2003-2017.

2.2.2 Microwave Limb Sounder (MLS)

The Earth Observing System (EOS) Microwave Limb Sounder (MLS) is aboard NASA's EOS Aura satellite flying in a polar sun-synchronous orbit. The EOS Aura MLS provides water vapor measurements from radiances measured primarily by the 190 GHz radiometer. The spatial coverage is near-global: 82° S degrees to 82° N latitude, with each profile spaced 1.5 degrees or ~165 km along the orbit track (~15 orbits per day). It performs 240 limb scans per orbit with a footprint of ~6 km across-track and ~ 200 km along-track and thus provides ~ 3500 profiles per day. Its vertical resolution is 1.3 – 3.6 km from 316 – 0.22 hPa, and the useful vertical range is

between 316 and 0.00215 hPa. We used version 4.2, level 2 MLS water vapor data (https://acdisc.gesdisc.eosdis.nasa.gov/data/Aura_MLS_Level2/ML2H2O.004/) (Livesey *et al*., 2020) and the retrieval procedure is documented in Read *et al.* (2007) and Lambert *et al*. (2007). We select the MLS daily profiles if they are located within 500 km of one the two selected radiosonde stations. MLS averaging kernel is applied on ERA-Interim water vapor data only when it is compared with MLS measurements. We have used all the quality measures described in the MLS data quality document (https://mls.jpl.nasa.gov/data/v4-2_data_quality_document.pdf). We have used all ERA-Interim reanalysis, regardless of whether MLS measured at South Asian stations. ERA-Interim, MLS or AIRS observation is considered temporally coincident when it occurs on the same calendar day as a radiosonde measurement.

2.2.3 ERA-Interim reanalysis

We analyze ERA-Interim specific humidity and potential vorticity (PV), (PVU, 1 PVU = 10^{-6} K m^2 $kg^{-1}s^{-1}$) for the period 1979 to 2017 (at 0.75° x 0.75° spatial and 6 hour time resolution) (Dee *et al.*, 2011) to understand its variability in the UTLS associated with DTs (https://apps.ecmwf.int/datasets/data/interim-full-daily/levtype=sfc/). Daily mean is obtained from 6 hourly data are analyzed on grid points centered at the two radiosonde stations considered in this study. The vertical resolution is sufficient in the UTLS (300-50 hPa) (300, 270 240, 215, 190, 165, 140, 122, 100, 87 73, 60, 50 hPa) to capture the vertical gradients in water vapor. Water vapor concentrations are estimated from specific humidity.

In the discussion that follows, seasons are considered as winter (December-January-February), pre-monsoon (March-April-May), monsoon (June-July-August-September) and post-monsoon (October-November). Over the South Asian region, ERA-Interim underestimates H_2O by 0.6 – 1.7 ppmv (14 – 30 %) at the pressure levels 400 – 30 hPa in comparison with balloon-borne cryogenic frostpoint hygrometers (CFH) measurements (Brunamonti, *et al*., 2019). ERA-Interim water vapor also differs against MLS in the UTLS (Jiang *et al*., 2015). Water vapor mixing ratios extracted on DT and ST days. We show the variation (DT-ST) of water vapor, temperature, PV, cloud occurrences (DCC,CC), cloud top height, and trends in water vapor at altitude relative to tropopause (TR1) since relative altitude is a better coordinate for examining the transition from the troposphere to the stratosphere (Pan *et al*., 2007).

The seasonal frequency of DT/ST days (%) when stratified for VDCC/DCC/CC is obtained as: ((occurrence frequency of DT/ST days associated with VDCC/DCC/CC in a particular season) / (total numbers of available DT/ST days of observation in that season))*100. The annual frequency is obtained as: (occurrence frequency of DT/ST associated the VDCC/DCC/CC divided by annual number of available observations)*100. The seasonal frequency of DT/ST days associated cloud with top height above the tropopause (%) is obtained as – ((number of DT/ST days associated with cloud top height above the tropopause in a particular season)/ (total numbers of available DT/ST days of observation in that season))*100). This computation is performed at the two stations at -5 to -3 km, -3 to -2 km, -2 to -1 km, -1 to 0 km, 0 to 1 km, 1 to 2 km, 2 to 3 km tropopause-relative altitude ranges. The relative changes in the frequency distribution of DT days with respect to ST days are presented for VDCC/DCC/CC occurrences and cloud top height.

2.2.4 Regression analysis

To estimate trends in water vapor (from ERA-Interim reanalysis), we use multiple regression analysis monthly time series at each given altitude following Randel and Cobb (1994) and Fadnavis and Beig (2006). The general expression for the regression model equation can be written as follows:

$$\theta(t) = \alpha(t) + \beta(t) * t + \gamma(t)QBO(t) + resid(t) \quad \textbf{(1)}$$

where θ(*t*) is a temperature time series at altitude. The model computes α, β, and γ using the harmonic expansion. The harmonic expansion for α(*t*) is given as

$$\alpha(t) = A_0 + A_1 \cos\omega t + A_2 \sin\omega t + A_3 \cos 2\omega t + A_4 \sin 2\omega t \quad \textbf{(2)}$$

where ω=2π/12; A_0, A_1, A_2 are constants and t is the time index (t=1,2,….n). α, β, and γ are calculated at every altitude; hence they are altitude dependent in expression (1). As a QBO proxy, QBO(t), we use Singapore monthly-mean QBO zonal winds (m/s) at 70 hPa (https://www.geo.fu-berlin.de/met/ag/strat/produkte/qbo/singapore.dat). Here, $\beta(t)$ and $\gamma(t)$ are the trend and QBO coefficients respectively, and resid(*t*) represents the residual or noise. Time series plots of α, β, γ and resid obtained from regression fitting on water vapor data for DT days at TR1 at Delhi are shown in figure S3. The monthly mean trend ($\beta(t)$) estimated from the model yields are used to obtain trend per decade (ppmv/decade). Error estimates are according to Neter *et al.* (1985) which can be represented by the following expression:

$$\sigma^2(\alpha) = [\sigma^2(A_0) + \sigma^2(A_1)cos^2\omega t + \sigma^2(A_2)sin^2\omega t \ldots\ldots$$

$$+2(\sigma(A_1A_2)cos\omega t + \sigma(A_1A_3)sin\omega t \quad \textbf{(3)}$$

293 Here $\sigma^2(A_0)$ and $\sigma(A_1A_2)$ and so on are variance-covariance estimates of regression coefficients,
294 obtained from least squares analysis (Randel and Cobb, 1994). The significance of the trend is
295 shown at the 95% confidence interval.
296
297 **3. Results**
298 **3.1. Characteristic features of double tropopauses**
299
300 Figures 2a-b show the monthly variation (composite of 1977 – 2017) of the relative
301 frequency of occurrence of DT days (%), and altitude (km) of TR1 and TR2 at two sub-tropical
302 South Asian stations, (1) Gauhati, and (2) Delhi. It is quite evident that monthly variations of the
303 frequency of occurrence of DT days and altitudes of TR1 and TR2 show a considerable seasonal
304 variability at Delhi and Gauhati, the north and north-east stations in South Asia. At these stations,
305 the frequency of occurrence of DT days is high during winter and pre-monsoon seasons (> 25 %)
306 and comparatively low during the monsoon season (5 – 15 %). Monthly mean altitudes of TR1 and
307 TR2 show a peak during monsoon season over: Delhi (TR1: 15.8 – TR2: 17.7 km), Gauhati (TR1:
308 15.6 – TR2: 17.5 km). The single tropopause (ST) lies between TR1 and TR2. The vertical extent
309 of the layer between DTs varies with the season and station. It is thicker during winter and pre-
310 monsoon seasons at Delhi (~3 – 4.5 km) and Gauhati (2 – 4 km). Interestingly, Fig. 2a-b also
311 shows that, in the months when the frequency of occurrence of DT days is high, the separation
312 between the two tropopauses increases. Peevey *et al*. (2012) also reported similar variation in
313 frequency of DTs and the distance between them.
314

Figures 2c-d show a seasonal variation of the temperature of TR1, TR2 and ST. TR1 is warmer than TR2 at Gauhati throughout the year while and the same is true at Delhi except for the monsoon season (in July-August TR2 is warmer than TR1). At both stations, temperature of ST lies between TR1 and TR2 except for the monsoon season (June-October). In the monsoon season, temperature of ST is closer to TR1 at Delhi and at Gauhati, it dangles near TR1 and TR2. Daily variation of temperature and height of ST, TR1 and TR2 indicates that TR1 is closer to ST (Fig S3). There may be migration of ST to TR1 and vice-a-versa before and after the DT (discussed in section 3.3) The temperature difference TR1-TR2 at these stations varies from ~ -2 to 13 K. The largest difference in temperature is seen during the winter/pre-monsoon seasons at Delhi and Gauhati. Temperature variations may be influenced by convective transport of warm-moist tropospheric air or driven by meridional migration of the boundary between tropical and extratropical air (Randel and Jensen, 2013; Fadnavis and Chattopadhyay, 2017) (discussed in section 3.3). Also, there may be influence of seasonal cycle of shortwave downwelling radiation (Donohoe and Battisti 2013). Daily radiosonde observations at Guahati (1984 –2017) and Delhi (1977-2017) show that DTs persist for 3-9 days (also see Fig. S4). Furtther, analysis of numbers of occurrences of DTs persisting for period varying between 1-9 days shows that beigest numbers of DTs persisted for 2-3 at Gauhati and Delhi (FigS5).

3.2 Variability of water vapor near the DTs

In the past, the satellite observations have shown a strong seasonal cycle in water vapor in the double tropopause region (Schwartz *et al.*, 2015). In-situ measurements have also shown that examples of extremes observed near a few convective events during DTs events (60 –225 ppmv compared to 5 – 10 ppmv in background) above the tropopause (Homeyer *et al*., 2014). Figure

3a-b shows water vapor mixing ratio difference profiles (DT-ST) from ERA-Interim (composite of 1980 – 2017) versus altitude relative to the first tropopause (TR1) at two South Asian stations for August (representative of monsoon season) and December (representative of the winter season). We show monthly variation instead of seasonal means because of monthly variability in the altitude of lower tropopause (TR1). Figure 3a-b depicts the enhancement of water vapor in the UTLS during both August and December at both stations. At these stations, the water vapor enhancement below the primary tropopause is larger in August than December. The range of enhancement of water vapor at Delhi and Gauhati, at 0 – 5 km below the tropopause is ~5.8±3.2 – 161.0±52 ppmv in August and 7.40±1.1 – 115.0±88.0 ppmv in December. Figures 3 c-d focus on 0 – 5 km above the tropopause for August and December, respectively. It shows that at 0 – 3.5 km above the tropopause, there is water vapor enhancement of 0.07±0.03 – 5.8±3.2 ppmv in August and 0.04±0.08 – 7.4±1.1 ppmv in December. However, at Delhi, the water vapor enhancement reduces to 0.02±0.03 ppmv during December near 5 km above the relative tropopause.

Figure 4 a-d shows MLS profiles of water vapor for DT-ST at both South Asian stations during August and December. At Delhi and Gauhati, the range of water vapor enhancement in the upper troposphere (0-5 km below the relative tropopause) in August is 3.0 ±3.6 to 410±150 ppmv; and December ~0.9±0.8 to 130±15 ppmv. In the layer 0.5 – 3.5 km above the tropopause, water vapor is enhanced by ~0.5±0.1 – 5.0±0.5 ppmv in August and 0.1±0.05 – 3.0±0.8 ppmv (except Delhi at 1.5 - 3 km) in December. In general, water vapor mixing ratios are higher in MLS than ERA-Interim in the upper troposphere. The differences in values may be due to lack of assimilated observations and deficiencies in the representation of transport in reanalysis may result in much poorer agreement amongst observational and reanalysis estimates (Davis et al., 2017).

3.3 Variability of potential vorticity near the DTs

Rossby wave breaking (RWB) plays an important role in formation of DTs (Pan et al 2009). Past studies show that poleward RWB carries subtropical upper tropospheric moist air into the extra-tropical lower stratosphere resulting in DT formation in the extra-tropical UTLS (Pan *et al.*, 2009; Ploeger *et al.*, 2013, Peevey *et al*., 2014). RWB can be identified from PV distribution at 350 K (Strong and Magnusdottir, 2008; Samanta *et al.*, 2016). RWB is manifested by the rapid and large-scale irreversible overturning of PV contours on isentropic surfaces (McIntyre and Palmer, 1985; Strong and Magnusdottir, 2008). The tropospheric air masses are identified as PV< 1 PVU and stratospheric air masses with PV> 2 PVU. Excursion of mid-latitude stratospheric air mass enhances PV values (PV>2PVU) over the tropical UTLS. While, poleward transport of tropical air (PV<2PVU) to the extratropics reduces PV values in the UTLS (Pan et al. 2009; Peevey et al. 2014; Fadnavis and Chattopadhyay 2017).

We show the distribution of potential vorticity (PV) on the 350 K potential surface on DT days to understand the influence of tropical tropospheric air masses on the extra-tropics and vice versa in Fig. 5a-d. It shows migration of low latitude air mass with low PV and enhanced water vapor to the extra-tropics (~50 ^{o}N) on one DT day in winter and one in summer. Simultaneously there is excursion of extra-tropical air mass to northeast India (90^{o}E, 23^{o}N). Ploeger et al. (2013) has also shown transport of water vapor from the tropics to extra-tropics. Similar transport between tropics and extra-tropics is observed in distribution of PV and water vapor during all DT days at Guahati and Delhi. Pan et al (2009) show that DTs at the mid-latitude are generated by migration of tropical tropospheric air mass above the tropopause of mid-latitude (Pan et al., 2009, Figure 1 therein). Similar transport from tropics to extra-tropics seems to be producing DTs over the subtropical South Asia (see Fig 5 a-d). The tropical air mass may be pushing down TR1 below its

normal position (Position of ST). This may be the reason that daily variation of altitude of TR1 shows it is slightly below the ST (Fig. S4 a-h). This indicates that there may be transition of TR1 to ST or vice-a-versa before and after the DT event. Figure 5 e-h shows the vertical variation of PV at tropopause-relative altitude. It also shows lower values of PV during DT days than ST days. It also indicates transport of low latitude air in the UTLS over extra-tropical South Asia during DT days.

3.4 Association of DTs with deep convective clouds

In this section, we explore the association of DTs with convective clouds. Previous studies have shown that DTs are formed in the regions of enhanced synoptic activity (Schmidt *et al*. 2006; Pan *et al*. 2009; Wang and Polvani, 2011; Peevey *et al.*, 2012; 2014). In South Asia, seasonally varying instability modulates the frequency of clouds reaching the upper troposphere within a few kilometers of the tropopause (Jensen and Del Genio, 2003; Bhawar *et al.*, 2014).

To understand the association of DTs with the convective cloud, we analyze cloud-top pressure (CTP) and temperature (CTT) at the station for every DT day. Our analysis shows clouds with CTP < 400 hPa and CTT < 235 K are present on ~52 – 78 % of the DTs days during 2003 – 2017. This indicates the tendency for convective clouds to be present on DTs days . A previous study based on CALIPSO observations reports that high altitude clouds over India have CTP < 400 hPa (> 8 km) (Meenu *et al.*, 2010). DT and ST days in a given season (seasonal frequency) are stratified as per occurrence of very deep convective clouds, deep convective cloud, and convective cloud(see Sect. 2.2.1). Table-1 shows the difference between the seasonal frequency of DT (%) and ST days (%) associated with very deep convective cloud (VDCC), deep convective

clouds (DCC) and convective clouds (CC) at two South Asian stations (significant at 95 % confidence interval). It indicates that higher frequency of DTs days than ST days at the stations is associated with VDCC and DCC during all these seasons. (One exception is Gauhati in pre-monsoon season where the frequency of DT days associated with DCC are lower than ST days). To understand the connection of water vapor and temperature variations with deep convection, we show frequency distribution of DT-ST days associated with convective clouds for the months August and December in Table S1. The distribution in these months is similar to the seasonal variation shown in Table-1.

Figure 6 a-b shows the frequency of DT and ST days (seasonal mean) when stratified by cloud top height at -5 to -3 km, -3 to -2 km, -2 to -1 km, -1 to 0 km, 0 to 1 km, 1 to 2 km, 2 to 3 km tropopause-relative altitude ranges. It shows that the frequency of DT days are associated with clouds tops reaching above the tropopause is higher than ST days at both stations and seasons. The frequency of DT days associated with clouds above the tropopause is higher at Delhi than Gauhati. The frequency distributions for the months of August and December are shown in Fig. S4.

4. Linkages between the variations of water vapor, temperature and convective clouds

Convection acts as an agent for transporting water vapor in the upper troposphere. The gravity waves generated from convection propagate into the stratosphere and enhance the vertical transport of water vapor to the stratosphere (Lane and Sharman, 2006). Water vapor enhancement for DT compared to ST days, between -5 and +5 km relative to the first tropopause may be due to transport via convective clouds associated with DT days (Table-1 and Fig. 6c-f) during 2003-2017.

In the UTLS, there may be horizontal transport of tropical moist air to subtropical South Asia due to Rossby wave breaking (Ploeger *et al*., 2013). Rossby wave breaking events may play an important role since they are associated with enhanced convection (Matthews and Kiladis 2000) and horizontal transport of tropical air masses to the extra-tropics (see Fig. 5a-d) (Ploeger *et al*., 2013). Past studies indicate that DTs can enable deeper convective overshooting of the tropopause and potentially inject higher amounts of water vapor (if the lower stratospheric stability is reduced compared to normal) (Homeyer *et al*., 2014;Schwartz *et al*., 2015; Solomon *et al*., 2016). Based on their analysis of humidity from Microwave Limb Sounder, Zhu *et al.* (2000) have also reported that the enhancement of moisture in the tropical upper troposphere is mainly by intensified local convection while the contribution of background fluxes and horizontal transport is relatively small. All South Asian stations show a higher frequency of DT days associated with cloud top height above the tropopause (~0 – 3 km) than ST days during all the seasons (Fig.6 and Fig. S6). It indicates that convective clouds near the tropopause may be enhancing water vapor in that region. The meridional transport from low latitude in the UTLS over South Asia has also been observed in profiles of potential vorticity (Fig. 5e-h). Further, we compute the composite of water vapor for DT (relative to TR1) and ST days associated with convective clouds (CC, DCC and VDCC together) (referred to as convective days) and days associated with no convective clouds (refereed as non-convective days). The difference in water vapor for convective days and non-convective days for the months of August and December is plotted in Fig. 6(c)-(f). It shows that enhancement of water vapor 0.06±0.04 to 16.2±6.5 ppmv below the relative tropopause and 0.04±0.02 to 0.18± 0.06 ppmv above the relative tropopause. This suggests that convective clouds might transport water vapor above the tropopause.

5. A long-term trend in the occurrence of DTs and associated water vapor in the UTLS

In this section, we provide estimates of trends in the occurrence of DTs and associated water vapor**.** Figure 7a shows trend values in the occurrence frequency of DT days (%) at the two stations. These stations show a positive (rising) trend in the occurrence of DT days with a rate of increase of ~0.27±0.12 to 0.4±0.2 % yr^{-1} (significant at 95 % confidence interval). From reanalysis and radiosonde data, Xian and Homeyer (2019) also observed an increase in frequency of occurrence of double tropopauses globally. Past studies show that hydration of the lower stratosphere from convection within DT environments can be significant (Homeyer *et al*., 2014; Schwartz *et al.*, 2015; Solomon *et al*., 2016). Figures 3-4 also show higher amounts of water vapor on DT days than ST days in the UTLS (except Delhi near 1.5 – 3 km above the relative tropopause in MLS data). We analyze trends in water vapor for DT and ST days near the tropopause (between +5 and -5 km relative to lower tropopause) from ERA-Interim reanalysis (Fig. 7b-c). The MLS period (2004 – 2016) used in this study is short for the long-term trend analysis and it has low number of overpasses at the two stations. Khosrawi et al. (2018) showed that MLS water vapour has significant drifts relative to MIPAS (depending on which MIPAS retrieval) and with some other sensors as well at low latitudes at 80 hPa which may show biases in trends. Therefore, trends estimates are shown from ERA-Interim data. A trend coefficient is obtained from monthly mean time series of DT and ST days separately. The estimated trend in water vapor for DT (ST) days is 20.2±11.3 to 0.15±0.09 ppmv/decade (7.9±4.3 to 0.04±0.03 ppmv/decade) below the tropopause (-5 to 0 km relative to lower tropopause). Above the tropopause (0 to +5 km relative to lower tropopause), it is 0.04±0.02 to 0.26±0.24 to ppmv/decade (0.02±0.01 to 0.08±0.05 ppmv/decade). The AIRS data (2002 – 2012) shows an increasing trend in frequency of occurrence of deep convective clouds (+1.05 ± 0.29% over the Indian Ocean and +3.15 ± 0.030% over Indian land (Aumann and Ruzmaikin, 2013). The increase in frequency of deep convection is associated with

surface warming. Thus, the occurrence frequency of double tropopauses may be a result of the warming environment of South Asia (Aumann *et al.*, 2018). These double tropopause events are associated with deep convective clouds injecting anomalously high water vapor in the UTLS (+5 to -5 km relative to the lower tropopause) and there may be horizontal transport of water vapor from the tropics to the subtropical UTLS (implied by Fig. 5).

6. Summary and discussions

This study presents variation of water vapor in the UTLS during the double tropopause events and its association with convective clouds over the sub-tropical South Asian region. Our analysis from multiple multi-decadal datasets (e.g. radiosonde temperature profiles during1984 – 2017 at Gauhati and 1977 – 2017 at Delhi), Atmospheric Infrared Sounder (2003 – 2017), and ERA-Interim reanalysis (1979 – 2017), Microwave Limb Sounder (2004 – 2016) shows that, in this region, deep convective clouds extend 2 – 3 km above the lower tropopause during DT days enhancing the anomalously high amount of water vapor in the altitude layer near the DTs. Additionally, there may be horizontal transport of water vapor from the tropics during Rossby wave breaking. Gravity waves excited from the convection may further enhance the vertical transport. The ERA-interim reanalysis shows that, during DT days, there is an enhancement of water vapor 5.8±3.2 to 161.0±52 ppmv below the tropopause and 0.007±0.03 – 7.4±1.1 ppmv above the lower tropopause in comparison with ST days. The analysis of water vapor co-located with convective clouds indicates enhancement of water vapor by 0.06±0.04 to 16.2±6.5 ppmv below the relative tropopause and 0.04±0.02 to 0.18± 0.06 ppmv above the relative tropopause on convective days relative to non-convective days. This indicates the role of convection in transporting water vapor above the tropopause.

A long-term analysis of radiosonde temperature profiles shows that DTs are occurring during all seasons of the year (frequency ~5 – 55 %). Occurrences of DTs show a rising trend at the subtropical South Asian stations (~0.27±0.12 to 0.4±0.2 %/year). The estimated trend in water vapor for DT (ST) days show linearly increase 20.2±11.3 to 0.15±0.09 ppmv/decade (7.9±4.3 to 0.04±0.03 ppmv/decade) below the tropopause (-5 to 0 km relative to lower tropopause). Above the tropopause, the trend is 0.04±0.02 to 0.26±0.24 ppmv/decade (0.02±0.01 to 0.08±0.05 ppmv/decade). Trends are estimated from ERA-Interim reanalysis and should be verified with water vapor measurements from balloon-borne measurements using cryogenic-frost-point-hygrometer at the South Asian stations considering the limitations of satellite measurements (revisit frequency, horizontal and vertical resolution, drifts, etc.). Our past study on comparison of balloon-borne measurements of water vapour with ERA-Interim data shows that ERA-Interim underestimates H_2O by 0.6–1.7 ppmv (14–30%) in the upper troposphere and lower stratosphere (200-30 hPa) (Brunamonti et al., 2019). While humidity measurements by Radiosonde RS41 show an average dry bias of 0.1–0.5 ppmv (3-9%) (Brunamonti et al., 2019). There is need for balloon borne water vapor measurements over South Asia considering the impact of the injection of water vapor into the stratosphere on climate change.

Over South Asia, rise in surface temperatures in the past 70 years lead to regional warming (1951 – 2013) (Ross *et al.*, 2018). The rising trend in the UTLS water vapor over subtropical South Asia may be a consequence of a warming environment. A recent study indicates that global warming has induced a rising trend in occurrence frequency of DT days globally (Xian and Homeyer, 2019). Also global warming has increased trends in deep convective clouds +1.05 ± 0.29 % yr^{-1} over the Indian Ocean and +3.15 ± 0.030 % yr^{-1} over the Indian lands (Aumann and Ruzmaikin, 2013). A rising trend in the water vapor in the UTLS will cause enhancement of long-wave radiation coming back down to warm the troposphere (Wang et al., 2017). A wetter

stratosphere produces stratospheric cooling and thinning of the ozone layer. The impacts of enhanced water vapor on radiative forcing are large and exacerbate global warming (Shindell 2001). It is important to reduce greenhouse gas concentrations to help avoid such negative consequences for the one billion inhabitants of South Asia.

Acknowledgment: The authors are thankful to Dr. Oolman, from University of Wyoming, for proving radiosonde data (http://weather.uwyo.edu/upperair/sounding.html), team members of ERA-Interim for meteorological data (http://apps.ecmwf.int/datasets/data/ interim-full-daily/levtype5pl/), AIRS (http://airs. jpl.nasa.gov/data/get_data), for cloud data and MLS (https://acdisc.gesdisc.eosdis.nasa.gov/data/Aura_MLS_Level2/ML2H2O.003/) foe water vapour data. Authors thank Felix Ploeger, Forschungszentrum Jülich, Jülich, Germany, for help related to MLS water vapor analysis.

References

Aumann, H. H., et al., 2003. AIRS/AMSU/HSB on the aqua mission: design, science objectives, data products, and processing systems. *IEEE Trans. Geosci. Remote Sens.*, **41**, 253–264, doi:10.1109/TGRS.2002.808356. http://ieeexplore.ieee.org/document/1196043/

Aumann, H. H. and A. Ruzmaikin. 2013. Frequency of Deep Convective Clouds in the Tropical Zone from 10 Years of AIRS Data. *Atmos. Chem. Phys*, **13**, 10795–10806, doi:10.5194/acp-13-10795-2013, www.atmos-chem-phys.net/13/10795/2013/

Aumann, H. H., et al., 2018. Increased Frequency of Extreme Tropical Deep Convection: AIRS Observations and Climate Model Predictions, *Geophys. Res lett*., **45**, 13,530–13,537. https://doi.org/10.1029/2018GL079423/

Bhawar, R. L., J. H. Jiang, H. Su, and M. J. Schwartz, 2014. Variation of upper tropospheric clouds and water vapor over the Indian Ocean. *Int. J. Climatol*., **34**, 3840–3848, doi:10.1002/joc.3942. http://doi.wiley.com/10.1002/joc.3942.

Brunamonti, S., L. Füzér, T. Jorge, Y. Poltera, P.Oelsner, S. Meier et al. 2019. Water vapor in the Asian summer monsoon anticyclone:Comparison of balloon-borne measurements and ECMWF data. *Journal of Geophysical Research, Atmospheres* **124**, 7053–7068. https://doi.org/10.1029/2018JD030000.

Castanheira, J. M., J. A. Añel, C. A. F. Marques, J. C. Antuña, M. L. R. Liberato, L. de la Torre, and L. Gimeno. 2009. "Increase of Upper Troposphere/Lower Stratosphere Wave Baroclinicity during the Second Half of the 20th Century." *Atmos. Chem. Phys Discussions* **9**(5):18597–619.

Davis, S. M, Hegglin M. I., Fujiwara M, et al. Assessment of Upper Tropospheric and Stratospheric Water Vapor and Ozone in Reanalyses as Part of S-RIP. *Atmos. Chem. Phys* Vol **17**.; 2017. doi:10.5194/ acp-17-12743-2017.

Dee, D. P., 2011. The ERA-Interim reanalysis: configuration and performance of the data assimilation system, *Q. J. R. Meteorol. Soc.* **137**, 553–597, DOI:10.1002/qj.828.

Dessler, A. E., M. R. Schoeberl, T. Wang, S. M. Davis, and K. H. Rosenlof. 2013. "Stratospheric Water Vapor Feedback." *Proceedings of the National Academy of Sciences of the United States of America* 110(45):18087–91.

Donohoe, A. and D. Battisti. 2013. The Seasonal Cycle of Atmospheric Heating and Temperature. *J .clim*, **26**, 4962-4980, dOI: 10.1175/JCLI-D-12-00713.1.

Fadnavis, S. and G. Beig. 2006. Seasonal Variation of Trend in Temperature and Ozone over the Tropical Stratosphere in the Northern Hemisphere. *Journal of Atmospheric and Solar-Terrestrial Physics*, **68** 1952–1961, doi:10.1016/j.jastp.2006.09.003.

Fadnavis, S., M. G. Schultz, K. Semeniuk, A. S. Mahajan, L. Pozzoli, S. Sonbawne, S. D. Ghude, M. Kiefer, and E. Eckert. 2014. Trends in Peroxyacetyl Nitrate (PAN) in the Upper Troposphere and Lower Stratosphere over Southern Asia during the Summer Monsoon Season: Regional Impacts. *Atmos. Chem. Phys*., **14**, 12725-12743, 2014a, doi.org/10.5194/acp-14-12725-2014a

Fadnavis, S., K. Semeniuk, L. Pozzoli, M. G. Schultz, S. D. Ghude, S. Das, and R. Kakatkar. 2013. Transport of Aerosols into the UTLS and Their Impact on the Asian Monsoon Region as Seen in a Global Model Simulation. *Atmos. Chem. Phys*., **13**, 8771-8786, http://doi.org/10.5194/acp-13-8771-2013

Fadnavis, S. and R. Chattopadhyay, 2017. Linkages of Subtropical Stratospheric Intraseasonal Intrusions with Indian Summer Monsoon Deficit Rainfall, *J. Clim*, **30**, 5083-5095, DOI: 10.1175/JCLI-D-16-0463.1.

Gettelman, A., D. E. Kinnison, T. J. Dunkerton, and G. P. Brasseur, 2004. Impact of Monsoon Circulations on the Upper Troposphere and Lower Stratosphere. *J. Geophys. Res. Atmos*., **109**, Doi10.10292004JD004878. ISBN 9781107445.Pdf.

Harrop, B. E., and D. L. Hartmann, 2015. The relationship between atmospheric convective, radiative effect and net energy transport in the tropical warm pool. *J. Clim*., **28**, 8620–8633, doi:10.1175/JCLI-D-15-0151.1.http://journals.ametsoc.org/doi/10.1175/JCLI-D-15-0151.1.

Homeyer, C. R., 2014. Convective Transport of Water Vapor into the Lower Stratosphere Observed during Double-Tropopause Events. *J. Geophys. Res. Atmos*., **119**, 10,910-941,958, doi10.10022014JD021485.

Homeyer, C. R., K. P. Bowman, and L. L. Pan, 2010. Extratropical tropopause transition layer characteristics from high-resolution sounding data, *J. Geophys. Res*., **115**, D13108, doi:10.1029/2009JD013664.

Ingram, W., 2010. A very simple model for the water vapour feedback on climate change, *Q. J. R. Meteorol. Soc*. **136**: 30–40. DOI:10.1002/qj.546.

Jensen, M. P., and A. D. Del Genio, 2003. Radiative and microphysical characteristics of deep convective systems in the tropical western Pacific. *J. Appl. Meteorol*., **42**, 1234–1254,

606 doi:10.1175/1520-0450(2003)042<1234:RAMCOD>2.0.CO;2.
607 http://journals.ametsoc.org/doi/abs/10.1175/1520-
608 0450%282003%29042%3C1234%3ARAMCOD%3E2.0.CO%3B2.

609 Jiang, J. H., H. Su, C. Zhai, L. Wu,K. Minschwaner, A. M. Molod, andA. M. Tompkins (2015), An
610 assessment ofupper troposphere and lower stratospherewater vapor in MERRA, MERRA2,
611 andECMWF reanalyses using Aura MLSobservations, *Journal of Geophysical Research, Atmospheres* **120**, 11,468–11,485, doi:10.1002/2015JD023752.
612
613 Kahn, B. H., F. W. Irion, V. T. Dang, E. M. Manning, S. L. Nasiri, C. M. Naud, J. M. Blaisdell, M.
614 M. Schreier, Q. Yue, K. W. Bowman, E. J. Fetzer, G. C. Hulley, K. N. Liou, D. Lubin, S. C.
615 Ou, J. Susskind, Y. Takano, B. Tian, and J. R. Worden. 2014. The Atmospheric Infrared
616 Sounder Version 6 Cloud Products. *Atmos. Chem. Phys*., **14**, 399-426, doi.org/10.5194/acp-
617 14-399-2014, http://www.atmos-chem-phys.net/14/399/2014/.
618 Kitchen M., 1989. Representativeness errors for radiosonde observations. Q. 1. R. Meteorol., 115,
619 pp. 673-700, 551.508.822: 53.088.
620 Khosrawi, F., et al , 2018. The SPARC water vapour assessment II: Comparison of stratospheric
621 and lower mesospheric water vapour time series observed from satellites *Atmospheric*
622 *Measurement Techniques*, **11(7)**: 4435-4463, http://dx.doi.org/10.5194/amt-11-4435-2018.
623 Lambert, A., and Coauthors, 2007. Validation of the Aura Microwave Limb Sounder middle
624 atmosphere water vapor and nitrous oxide measurements. *J. Geophys. Res*., **112**, D24S36,
625 doi:10.1029/2007JD008724.

626 Lane, T. P., and R. D. Sharman, 2006. Gravity wave breaking, secondary wave generation, and
627 mixing above deep convection in a three-dimensional cloud model, *Geophys. Res. Lett***., 33,**
628 L23813, doi:10.1029/2006GL027988.

629 Livesey N.J. et al, 2020, Version 4.2x Level 2 and 3 data quality and description document, JPL D-
630 33509 Rev. E , https://mls.jpl.nasa.gov/data/v4-2_data_quality_document.pdf.

631 Manney, G. L., M. I., Hegglin, Z. D. Lawrence, K. Wargan, L. F. Millán., M. J. Schwartz, L. S.
632 Michelle, A. Lambert, S. Pawson, B. W. Knosp, R. A. Fuller, and W. H. Daffer, 2017.
633 Reanalysis comparisons of upper tropospheric-lower stratospheric jets and multiple
634 tropopauses. *Atmos. Chem. Phys*., **17**, 11541-11566,doi: 10.5194/acp-17-11541-2017.

635 Manohar, G. K., S. S. Kahdalgaonkar, and M. I. R. Tinmaker. 1999. Thunderstorm Activity over
636 India and the Indian Southwest Monsoon. . *Geophys. Res*, **104**, D4, 4169-4188,

http://doi.org/10.1029/98JD02592

Matthews, A. J. and G. N. Kiladis. 2000. "A Model of Rossby Waves Linked to Submonthly Convection over the Eastern Tropical Pacific." *Journal of the Atmospheric Sciences* **57**(23):3785–98.

Meenu, S., K. Rajeev, K. Parameswaran, and Anish Kumar M. Nair. 2010. Regional Distribution of Deep Clouds and Cloud Top Altitudes over the Indian Subcontinent and the Surrounding Oceans. *J. Geophys. Res*., **115**, D05205, doi:10.1029/2009JD011802. http://doi.wiley.com/10.1029/2009JD011802.

Neter, J., Wasserman, W., Kunter, M.H., 1985. Applied Linear Statistical Models, second ed. Richard D Irwin, Homewood,IL, 1127 pp.

Pan, L. L., W. J. Randel, J. C. Gille, W. D. Hall, B. Nardi, S. Massie, V. Yudin, R. Khosravi, P. Konopka, and D. Tarasick. 2009. Tropospheric Intrusions Associated with the Secondary Tropopause. *J. Geophys. Res*., **114,** D10302, doi:10.1029/2008JD011374, http://doi.wiley.com/10.1029/2008JD011374..

Pan, L. L., Kenneth P. Bowman, M. Shapiro, W. J. Randel, R. S. Gao, T. Campos, C. Davis, S. Schauffler, B. A. Ridley, J. C. Wei, and C. Barnet. 2007. Chemical Behavior of the Tropopause Observed during the Stratosphere-Troposphere Analyses of Regional Transport Experiment. *J. Geophys. Res*., **112**, D18110, doi:10.1029/2007JD008645.

Peevey, T. R., J. C. Gille, C. R. Homeyer, and G. L. Manney. 2014. The Double Tropopause and Its Dynamical Relationship to the Tropopause Inversion Layer in Storm Track Regions. *J. Geophys. Res*., **119**, 10194 - 10212, doi:10.1002/2014JD021808.

Peevey, T. R., J. C. Gille, C. E. Randall, and A. Kunz, 2012. Investigation of double tropopause spatial and temporal global variability utilizing High-Resolution Dynamics Limb Sounder temperature observations. *J. Geophys. Res*., **117**, 1–14, doi:10.1029/2011JD016443.

Ploeger, F., G. Günther, P. Konopka, S. Fueglistaler, R. Müller, C. Hoppe, A. Kunz, R. Spang, J. U. Grooß, and M. Riese. 2013. Horizontal Water Vapor Transport in the Lower Stratosphere from Subtropics to High Latitudes during Boreal Summer. *J. Geophys. Res*., **118**, 8111–8127, doi:10.1002/jgrd.50636

Randel, J., Janel B. Cobb, and Abstract Space-time. 1994. Coherent Variations of Monthly and Lower Stratospheric Temperature (or (A ,, A2) Costa Sin. 99:5433–47.

667 Randel, W. J., and E. J. Jensen, 2013. Physical processes in the tropical tropopause layer and their
668 roles in a changing climate. *Nat. Geosci*., **6,** 169–176, doi:10.1038/ngeo1733.
669 http://www.nature.com/articles/ngeo1733.

670 Randel, W. J., D. J. Seidel, and L. L. Pan, 2007. Observational characteristics of double
671 tropopauses. *J. Geophys. Res*., **112**, D07309, doi:10.1029/2006JD007904.
672 http://doi.wiley.com/10.1029/2006JD007904.

673 Read, W. G., and Coauthors, 2007. Aura Microwave Limb Sounder upper tropospheric and lower
674 stratospheric H2O and relative humidity with respect to ice validation. *J. Geophys. Res*., **112**,
675 D24S35, doi:10.1029/2007JD008752.

676 Riese, M., F. Ploeger, A. Rap, B. Vogel, P. Konopka, M. Dameris, and P. Forster. 2012. "Impact of
677 Uncertainties in Atmospheric Mixing on Simulated UTLS Composition and Related Radiative
678 Effects." *J. Geophys. Res.*, **117**, D16305, doi:10.1029/2012JD017751.
679 http://doi.wiley.com/10.1029/2012JD017751

680 Roca, R., and V. Ramanathan, 2000. Scale dependence of monsoonal convective systems over the
681 Indian Ocean. *J. Clim*., **13**, 1286–1298, doi:10.1175/1520-
682 0442(2000)013<1286:SDOMCS>2.0.CO;2.
683 http://journals.ametsoc.org/doi/abs/10.1175/1520-
684 0442%282000%29013%3C1286%3ASDOMCS%3E2.0.CO%3B2.

685 Rolf, C, B. Vogel,P Hoor, A. Afchine, G. Günther, M. Krämer, R. Müller, S. Müller, N. Spelten,
686 and M. Riese, 2018. Water vapor increase in the lower stratosphere of the Northern
687 Hemisphere due to the Asian monsoon anticyclone observed during the TACTS/ESMVal
688 campaigns, *Atmos. Chem. Phys*., **18**, 2973-2983, https://doi.org/10.5194/acp-18-2973-2018

689 Ross, R. S., T. N. Krishnamurti, S. Pattnaik, and D. S. Pai, 2018. Decadal surface temperature
690 trends in India based on a new high-resolution data set. *Scientific Reports*, **8**:7452
691 |DOI:10.1038/s41598-018-25347-2.

692 Roxy, M. K., R. Kapoor, P. Terray, S. Masson, 2014. The Curious Case of Indian Ocean Warming.
693 Journal of Climate, *American Meteorological Society*, **27** (22), pp.8501-8509.
694 <10.1175/JCLI-D-14-00471.1

695 Roy, C., S. Fadnavis, R. Müller, D. C. Ayantika, F. Ploeger, and A. Rap, 2017. Influence of
696 enhanced Asian NOx emissions on ozone in the upper troposphere and lower stratosphere in

chemistry-climate model simulations. *Atmos. Chem. Phys*., **17**, 1297–1311, doi:10.5194/acp-17-1297-2017.

Sausen, R., and B. D. Santer, 2003. Use of changes in tropopause height to detect human influences on climate. *Meteorol. Zeitschrift*, **12**, 131–136, doi:10.1127/0941-2948/2003/0012-0131.

Schmidt, T., G. Beyerle, S. Heise, J. Wickert, and M. Rothacher. 2006. A Climatology a Multiple Tropauses Derived from GPS Radio Occultations with CHAMP and SAC-C. *Geophys. Res. Lett*., **33,** L04808, doi:10.1029/2005GL024600.

Schwartz, M. J., G. L. Manney, M. I. Hegglin, N. J. Livesey, M. L. Santee, and W. H. Daffer. 2015. Climatology and Variability of Trace Gases in Extratropical Double-Tropopause Regions from MLS, HIRDLS, and ACE-FTS Measurements. *J. Geophys. Res. Atmos*., **120**, 843–867, doi:10.1002/2014JD021964.

Shindell, D. T., 2001. Climate and ozone response to increased stratospheric water vapor. *Geophys. Res. Lett*. **28**, 1551-1554.

Solomon, D. L., K. P. Bowman, and C. R. Homeyer, 2016. Tropopause-penetrating convection from three-dimensional gridded NEXRAD data. *J. Appl. Meteor. Climatol*., **55**, 465-476, doi: 10.1175/JAMC-D-15-0190.1.

Solomon, S., K. H. Rosenlof, R. W. Portmann, J. S. Daniel, S. M. Davis, T. J. Sanford, and G.-K. Plattner, 2010. Contributions of stratospheric water vapor to decadal changes in the rate of global warming. *Science*, **327,** 1219-1223, doi: 10.1126/science.1182488.

Virts, K. S. and R. A. Houze JR, 2015. Clouds and Water Vapor in the Tropical Tropopause Transition Layer over Mesoscale Convective Systems. *Journal of the Atmospheric Sciences*, **72**, 4739-4753., doi: 10.1175/JAS-D-15-0122.1.

Wang, S. and L. M. Polvani. 2011. Double Tropopause Formation in Idealized Baroclinic Life Cycles: The Key Role of an Initial Tropopause Inversion Layer. *J. Geophys. Res*., **116**, D05108, doi:10.1029/2010JD015118.

Wang Y., Hui Su · Jonathan H. Jiang, · Nathaniel J. Livesey, · Michelle L. Santee, · Lucien Froidevaux, · William G. Read, · John Anders. 2017 The linkage between stratospheric water vapor and surface temperature in an observation-constrained coupled general circulation model, *Clim Dyn*., **48**,:2671–2683, DOI 10.1007/s00382-016-3231-3

Weisz, E., J. Li, W. P. Menzel, A. K. Heidinger, B. H. Kahn, and C.-Y. Liu, 2007. Comparison of AIRS, MODIS, CloudSat and CALIPSO cloud top height retrievals. *Geophys. Res. Lett.*, **34**, L17811, doi:10.1029/2007GL030676. http://doi.wiley.com/10.1029/2007GL030676.

WMO, World Meteorological Organization 1957: Meteorology — A three-dimensional science: Second session of the Commission for Aerology. WMO Bulletin, 4, 134–138.

Xian, T. and C. R. Homeyer, 2019. Global tropopause altitudes in radiosondes and reanalyses, *Atmos. Chem. Phys*., **19**, 5661–5678. https://doi.org/10.5194/acp-19-5661-2019.

Zhu, Y., R. E. Newell, and W. G. Read, 2000. Factors Controlling Upper-Troposphere Water Vapor, *J. Clim*, **13**, 836-848.

Table and Figure captions

Table-1: Distribution of seasonal and annual frequency difference (DT-ST days, %) associated with very deep convective clouds (VDCC; CTT < 210K), deep convective clouds (DCC; CTT = 220 – 235 K), and convective clouds (CC; CTT = 235 – 255 K) when CTP < 400 hPa at the Gauhati and Delhi during 2003 – 2017. The criteria of classification of clouds into categories of very DCC, DCC, and CC are adopted from Roca and Ramanathan (2000). The seasonal and annual frequency difference estimates are significant at 95% confidence interval.

FIG. 1.(a) A map showing two stations in the subtropical South Asia, Gauhati (26.10° N, 91.58° E), and Delhi (28.70° N, 77.10° E). Radiosonde and ERA-Interim (ERA-I) temperature profile at (b) Gauhati at 12 UTC on 3 December 2017, (c) Delhi at 00 UTC on 18 January 2013. First (TR1) and second (TR2) tropopauses are indicated by arrows.

FIG. 2. Monthly variation of frequency of occurrence (%) of DTs (bars), tropopause height (km) of TR1 (red) and TR2 (green) and single tropopause (ST) (black) at (a) Gauhati (26.14° N, 91.73° E) for January 1984 – December 2017, (b) Delhi (28.70° N, 77.10° E) for (January 1977 – December 2017). (c)-(d) same as (a)-(b) but for monthly mean tropopause temperature (K) of TR1, TR2 and ST. The horizontal line shows the standard deviation in Figs. (a)-(d).

FIG.3: Profiles of water vapor enhancement (DT-ST) [ppmv] from ERA-Interim (composite of 1980 – 2017) plotted for tropopause relative altitude (-5 to +5 km) at Gauhati and Delhi for (a) August (b) December, (c)-(d) are same as (a)-(b) but for 0 – 5 km above the tropopause. Horizontal lines on each profile indicate standard deviation.

FIG.4: Profiles of water vapor (DT-ST) [ppmv] from MLS (composite of 2004 – 2016) plotted for tropopause relative altitude (-5 to +5 km) at Gauhati and Delhi in (a) August (b) December, (c)-(d) are same as (a)-(b) but for 0 – 5 km above the tropopause. Horizontal lines on each profile indicate standard deviation.

FIG. 5. Distribution at 350 K potential temperature surface on 2 August, a double tropopause day for (a) potential vorticity (PVU, 1 PVU = 10-6 K m2 kg-1s -1), and (b) water vapor mixing rations (ppmv), (c) – (d) same as (a) – (b) but for 8 Dec 2016, a double tropopause day. In Figs (a)-(d) arrows indicate region of transport. Contour in Figs. (b) and (d) indicate 1PVU and 2 PVU lines. Profiles of potential vorticity (PV) (PVU, 1 PVU = 10-6 K m2 kg-1s -1) from ERA-Interim (composite of 1980 – 2016) plotted for tropopause relative altitude (-5 to +5 km) at Gauhati for (e) August, (f) December, (g)-(h) same as (e)-(f) but for Delhi. Horizontal lines on each profile indicate standard deviation.

FIG. 6: Seasonal variation of frequency (%) of DT and ST days (climatology 2003 - 2017) when stratified by cloud top height (km) (AIRS) for tropopause-relative altitude ranges of -5 to -3 km,

771 -3 to -2 km, -2 to -1 km, -1 to 0 km, 0 to 1 km, 1 to 2 km, 2 to 3 km at (a) Gauhati (26.14° N,
772 91.73° E) and (b) Delhi (28.70° N, 77.10° E). The difference in water vapor (ERA-Interim) for
773 convective days and non-convective days for (c) August plotted at tropopause relative altitude -
774 5 to +5 km , (d) same as (c) but for tropopause relative altitude 0 to +5 km, (e) same as (c) but
775 for December, (f) same (d) but for December. Horizontal lines in (c)-(f) indicate standard
776 deviation.

777 FIG. 7: (a) Trend (% /year) in occurrence of numbers of DT days at Gauhati (January 1984 –
778 December 2017) and Delhi (January 1977 – December 2017), (b) trend [ppmv/decade] in ERA-
779 Interim water vapor for the DT days during January 1980 – December 2017 at the altitudes
780 between -5 to +5 km relative to tropopause at Delhi and Gauhati, (c) same as (b) but for 0 to +5
781 km relative to tropopause, (d) same as (b) but for ST days, (e) same as (d) but for 0 to +5 km
782 relative to tropopause. Horizontal lines in (a) – (e) indicate standard deviation.

783

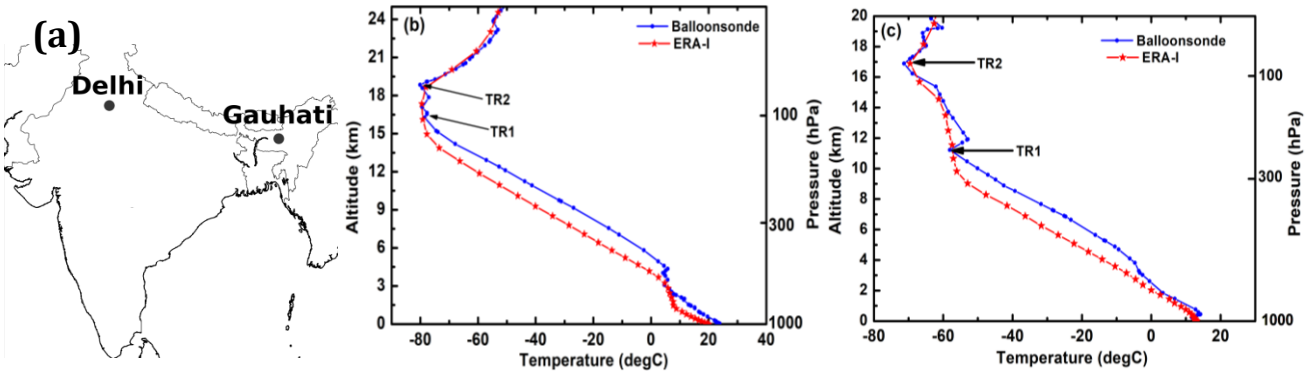

FIG. 1.(a) A map showing two stations in the subtropical South Asia, Gauhati (26.10° N, 91.58° E), and Delhi (28.70° N, 77.10° E). Radiosonde and ERA-Interim (ERA-I) temperature profile at (b) Gauhati at 12 UTC on 3 December 2017, (c) Delhi at 00 UTC on 18 January 2013. First (TR1) and second (TR2) tropopauses are indicated by arrows.

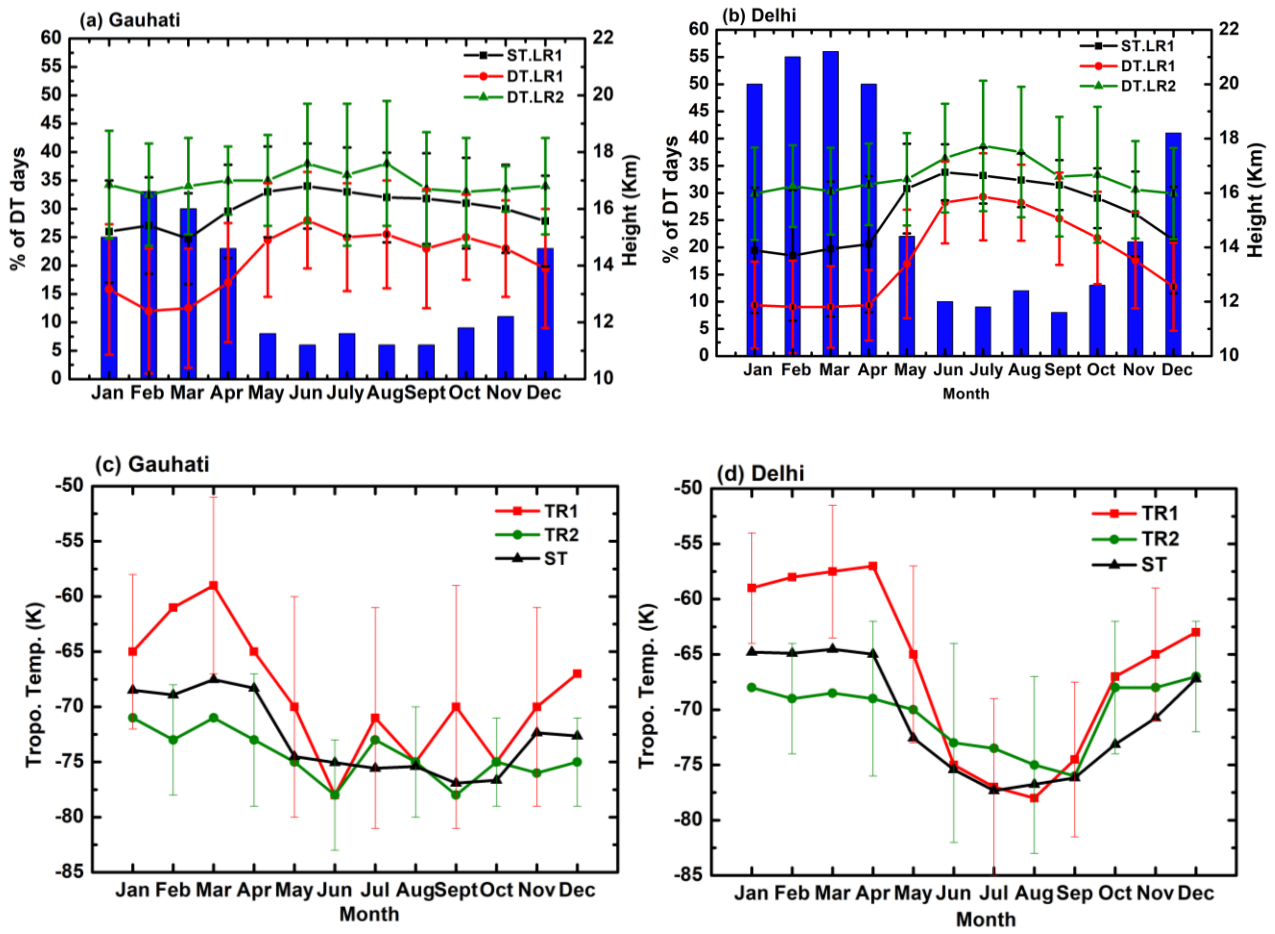

FIG. 2. Monthly variation of frequency of occurrence (%) of DTs (bars), tropopause height (km) of TR1 (red) and TR2 (green) and single tropopause (ST) (black) at (a) Gauhati (26.14° N, 91.73° E) for January 1984 – December 2017, (b) Delhi (28.70° N, 77.10° E) for (January 1977 – December 2017). (c)-(d) same as (a)-(b) but for monthly mean tropopause temperature (K) of TR1, TR2 and ST. The horizontal line shows the standard deviation in Figs. (a)-(d).

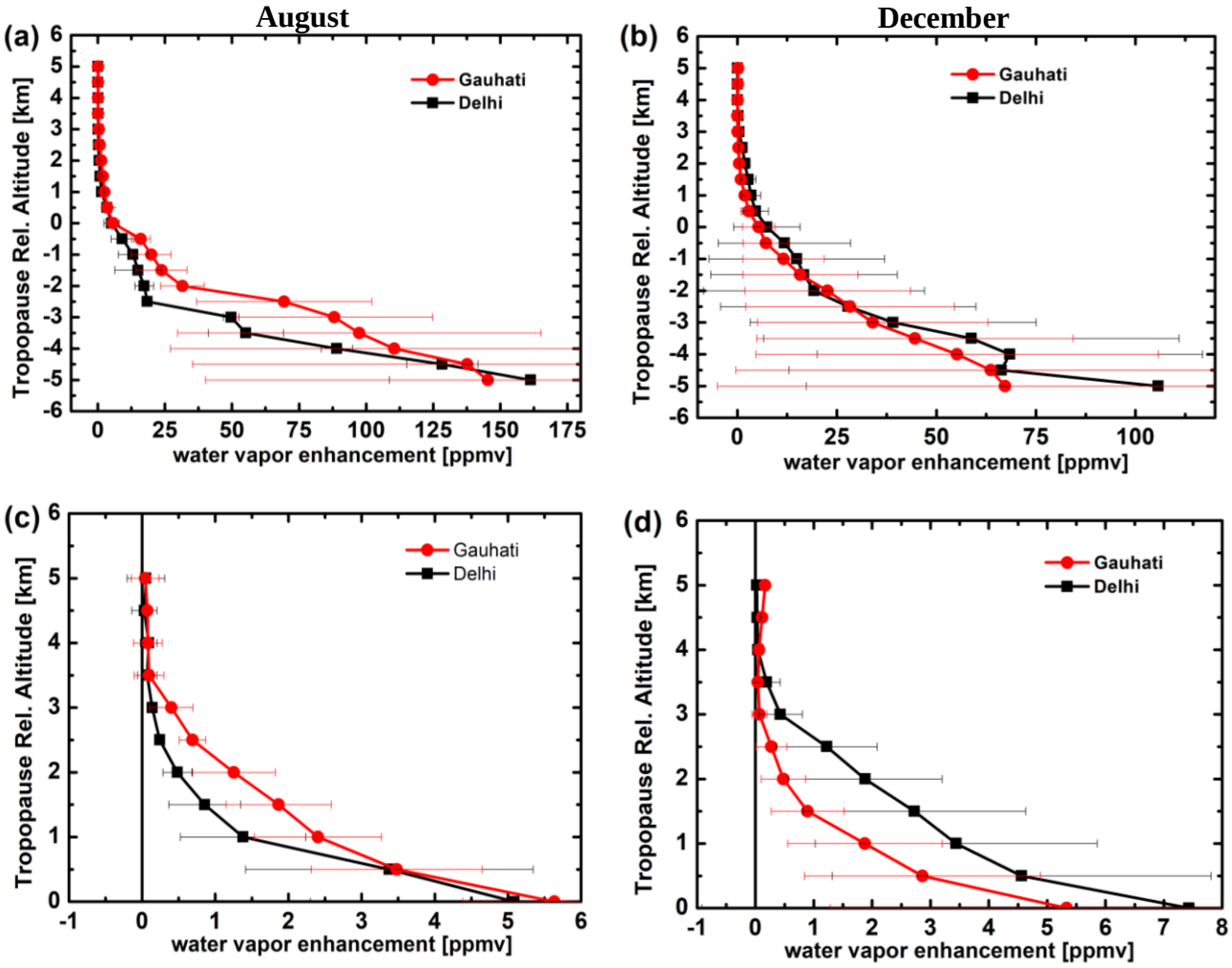

FIG.3: Profiles of water vapor enhancement (DT-ST) [ppmv] from ERA-Interim (composite of 1980 – 2017) plotted for tropopause relative altitude (-5 to +5 km) at Gauhati and Delhi for (a) August (b) December, (c)-(d) are same as (a)-(b) but for 0 – 5 km above the tropopause. Horizontal lines on each profile indicate standard deviation.

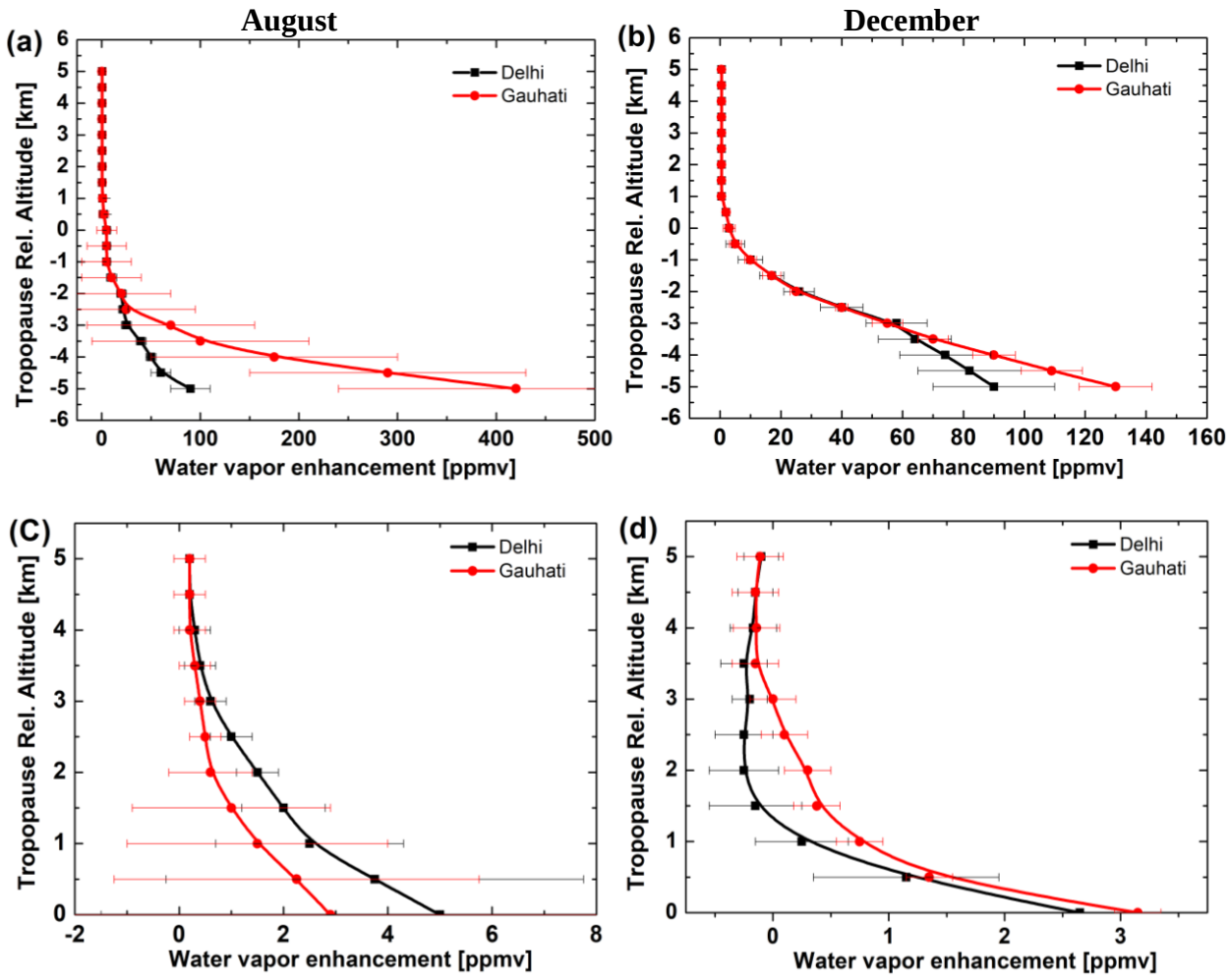

FIG.4: Profiles of water vapor (DT-ST) [ppmv] from MLS (composite of 2004 – 2016) plotted for tropopause relative altitude (-5 to +5 km) at Gauhati and Delhi in (a) August (b) December, (c)-(d) are same as (a)-(b) but for 0 – 5 km above the tropopause. Horizontal lines on each profile indicate standard deviation.

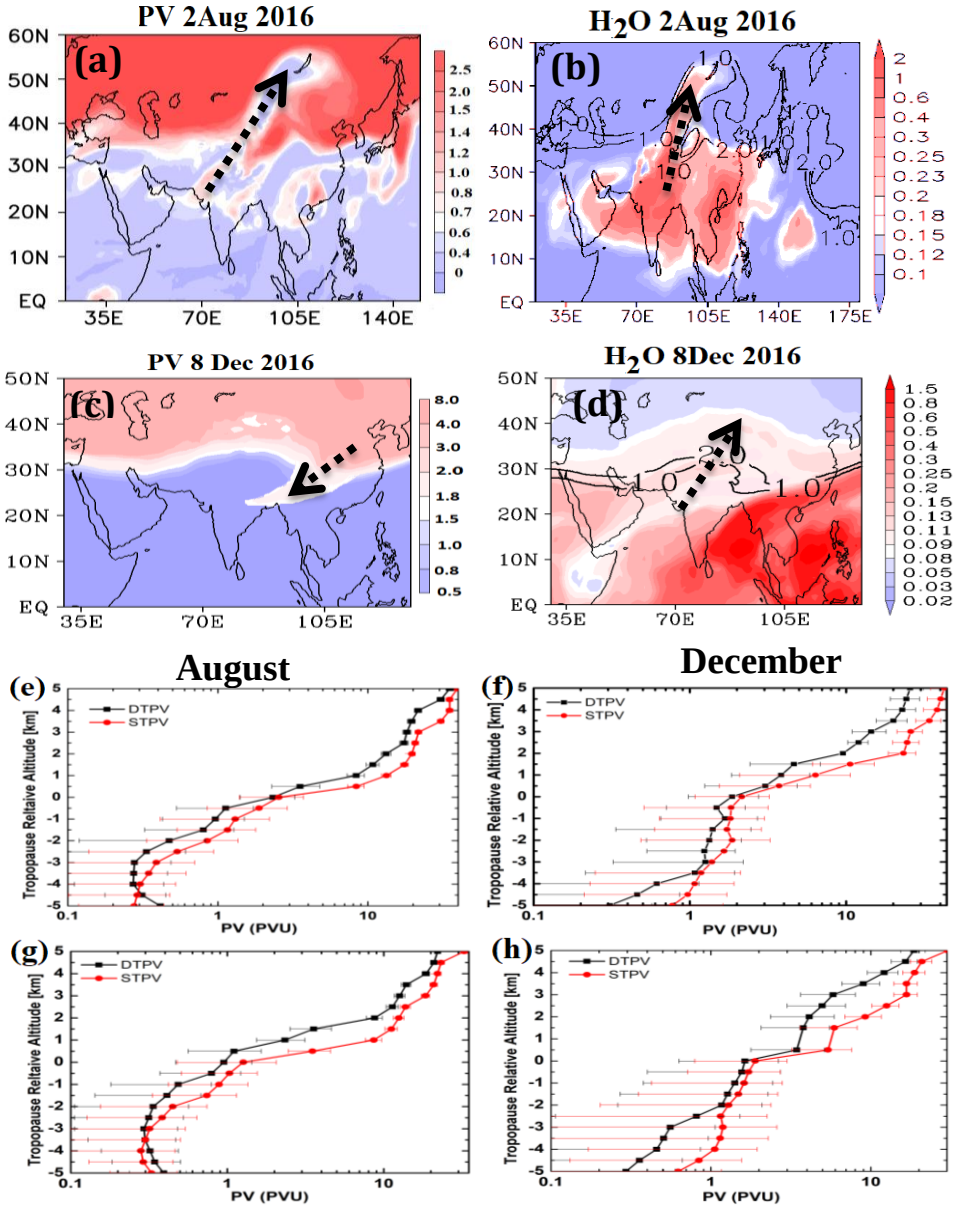

FIG. 5. Distribution at 350 K potential temperature surface on 2 August, a double tropopause day for (a) potential vorticity (PVU, 1 PVU = 10^{-6} K m^2 $kg^{-1}s^{-1}$), and (b) water vapor mixing rations (ppmv), (c) – (d) same as (a) – (b) but for 8 Dec 2016, a double tropopause day. In Figs (a)-(d) arrows indicate region of transport. Contour in Figs. (b) and (d) indicate 1PVU and 2 PVU lines. Profiles of potential vorticity (PV) (PVU, 1 PVU = 10^{-6} K m^2 $kg^{-1}s^{-1}$) from ERA-Interim (composite of 1980 – 2016) plotted for tropopause relative altitude (-5 to +5 km) at Gauhati for (e) August, (f) December, (g)-(h) same as (e)-(f) but for Delhi. Horizontal lines on each profile indicate standard deviation.

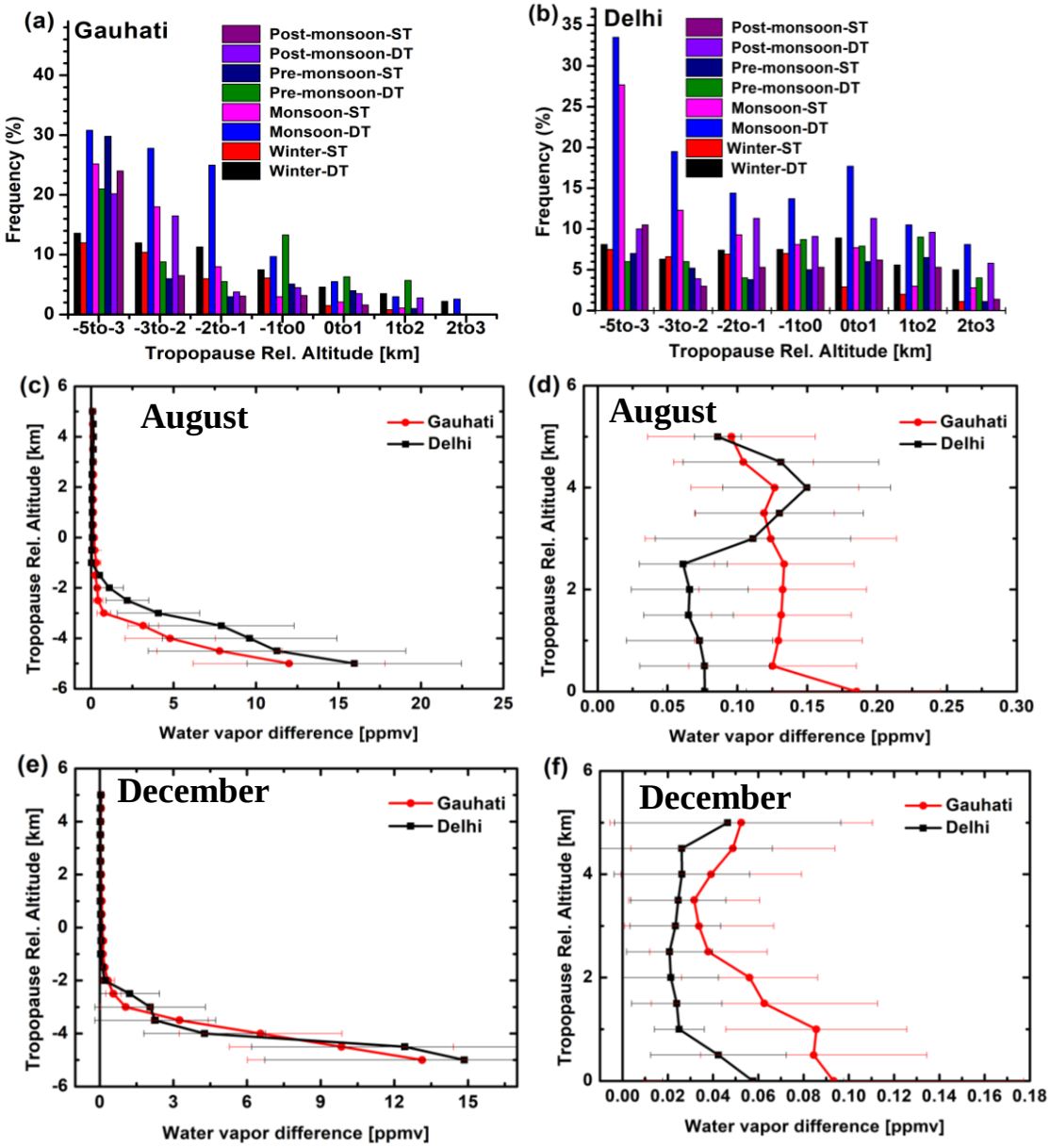

FIG. 6: Seasonal variation of frequency (%) of DT and ST days (climatology 2003-2017) when stratified by cloud top height (km) (AIRS) for tropopause-relative altitude ranges of -5 to -3 km, -3 to -2 km, -2 to -1 km, -1 to 0 km, 0 to 1 km, 1 to 2 km, 2 to 3 km at (a) Gauhati (26.14° N, 91.73° E) and (b) Delhi (28.70° N, 77.10° E). The difference in water vapor (ERA-Interim) for convective days and non-convective days for (c) August plotted at tropopause relative altitude -5 to +5 km , (d) same as (c) but for tropopause relative altitude 0 to +5 km, (e) same as (c) but for December, (f) same (d) but for December. Horizontal lines in (c)-(f) indicate standard deviation.

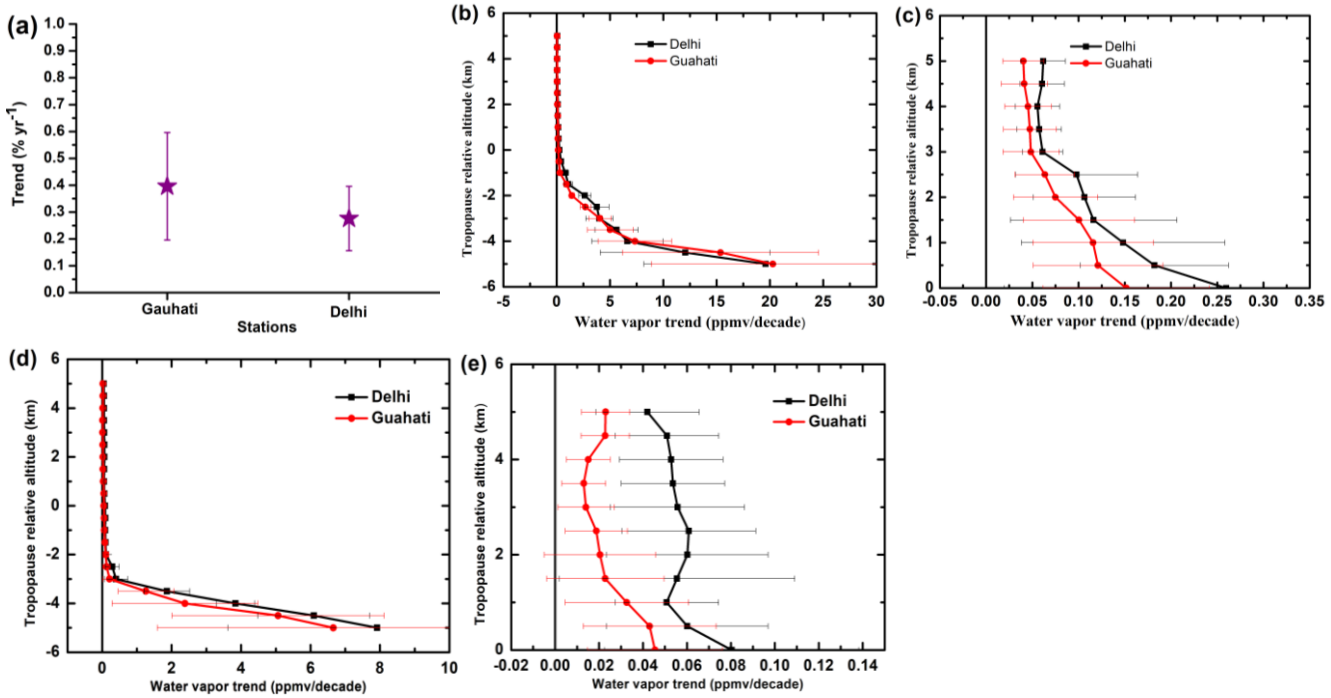

FIG. 7: (a) Trend (% /year) in occurrence of numbers of DT days at Gauhati (January 1984 – December 2017) and Delhi (January 1977 – December 2017), (b) trend [ppmv/decade] in ERA-Interim water vapor for the DT days during January 1980 – December 2017 at the altitudes between -5 to +5 km relative to tropopause at Delhi and Gauhati, (c) same as (b) but for 0 to +5 km relative to tropopause, (d) same as (b) but for ST days, (e) same as (d) but for 0 to +5 km relative to tropopause. Horizontal lines in (a)-(e) indicate standard deviation.

Supplementary Table and figures

Table S1: Distribution of frequency of DT-ST days (%) associated with deep convective clouds (DCC; CTT = 220 – 235 K), and convective clouds (CC; CTT = 235 – 255 K) when CTP < 400 hPa for the months of August and December at the two different stations over South Asia. Clouds are categorized as very DCC, DCC, and CC, following Roca and Ramanathan (2000).

Station	Month	VDCC	DCC	CC
Gauhati	Aug	2.6	14.85	3.25
	Dec	4.8	17.03	6.53
Delhi	Aug	8.1	1.08	14.74
	Dec	6.0	18.1	4068

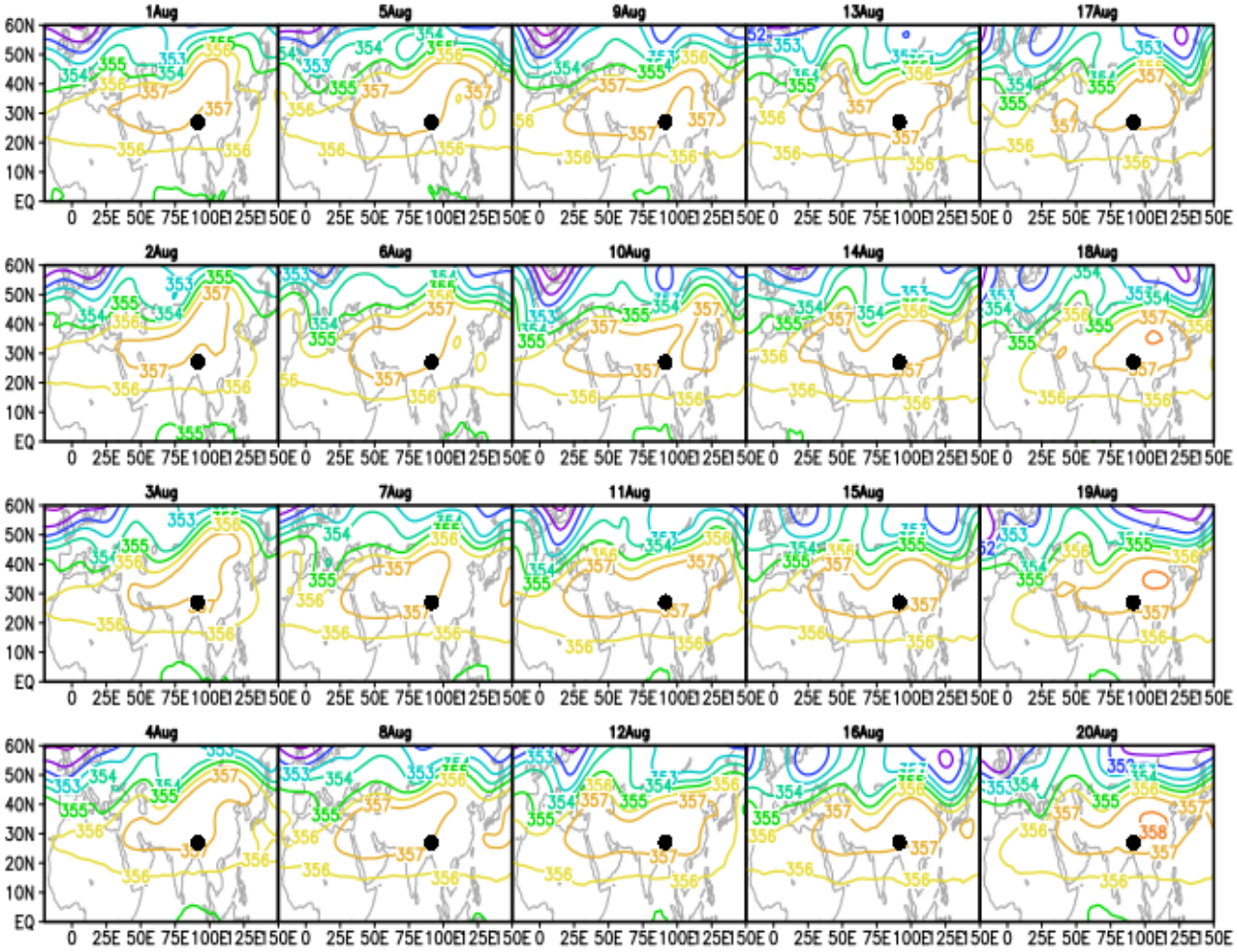

Figure S1: Distribution of Montgomery potential stream function at 350 K potential surface for 1-20 August 2016. A black dot indicates the location of Gauhati.

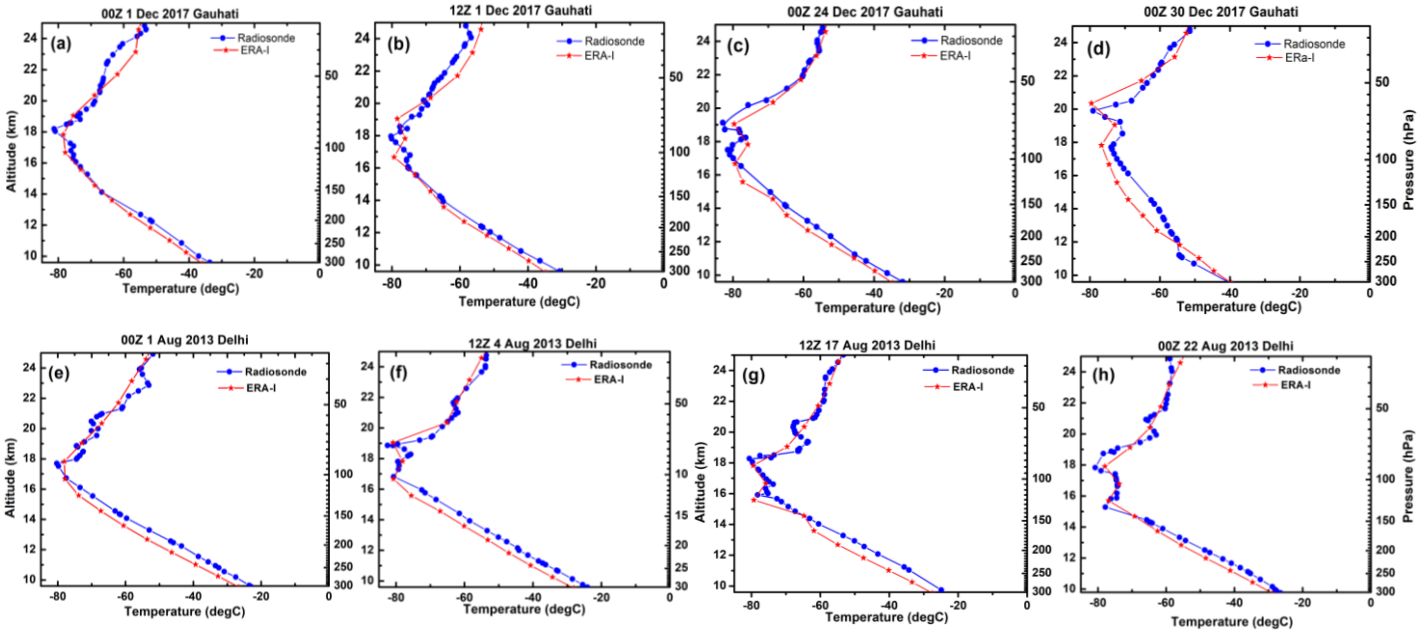

Figure S2: Vertical profiles of temperature from radiosonde and ERA-Interim for typical ST and DT days over Gauhati in December 2017 for (a)00Z 1 Dec, a ST day, (b) 12Z 1Dec a DT day, (c)00Z 24 Dec a DT day, (d) 00Z 30 Dec, a DT day, Delhi in August 2013 on (e) 00Z 1Aug,a ST day, (f) 4 Aug, a DT day, (g)12Z 17 Aug, a DT day, (h) 00z 22Aug,a DT day.

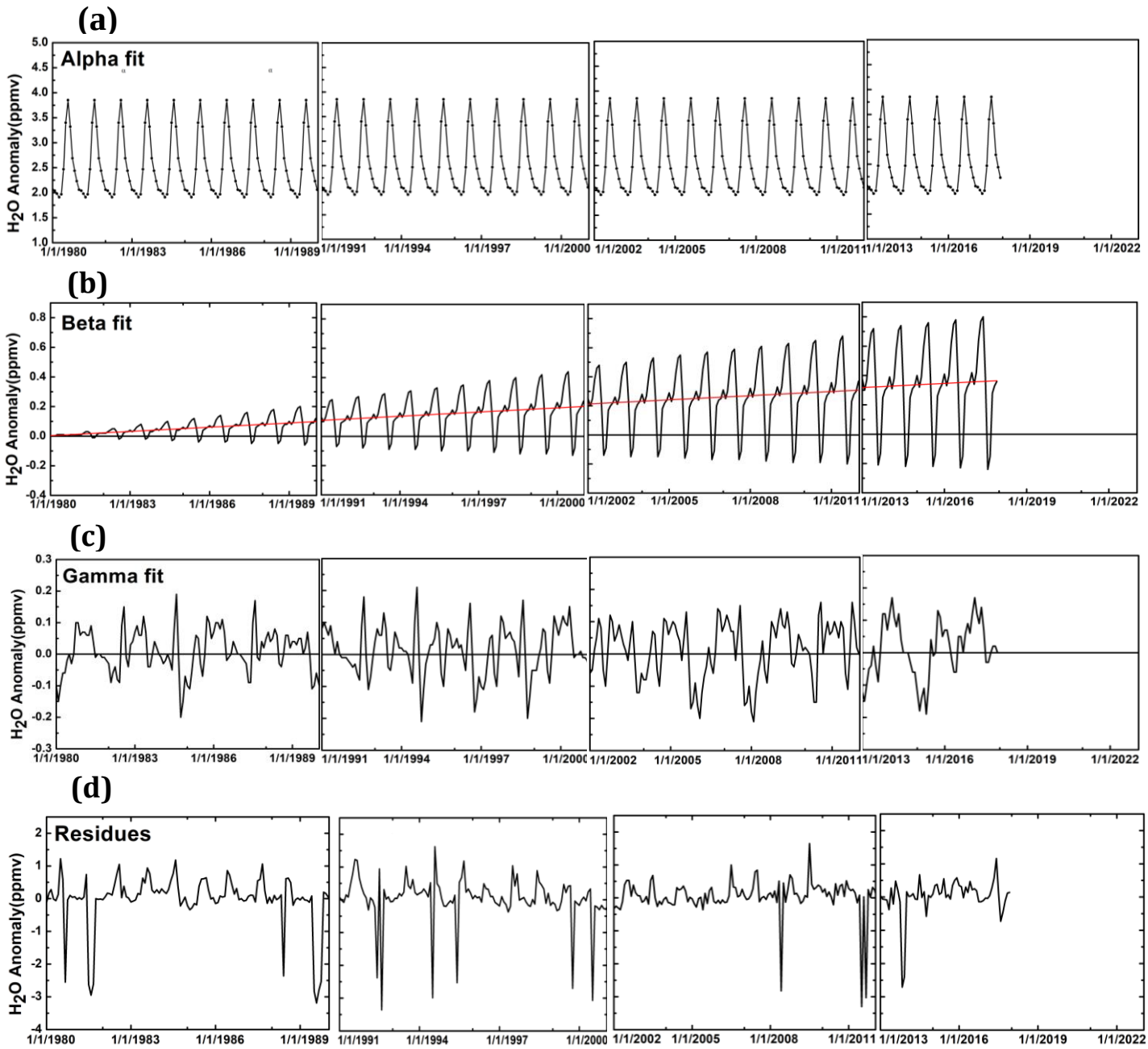

Figure S3: Plot of explained water vapor anomaly (ppmv) for each regression fit term at the lower tropopause on double tropopause days during 1-1-1980 to 31-12-2017 at Delhi for (a) α(alpha), the seasonal coefficient (including constant), (b) β (beta) the trend coefficient, (c) γ (gamma) the QBO coefficient, (d) Plot of residues from the sum of the fit terms (panels a-c) to the ERA-Interim time series. Red line in fig (b) indicates slope.

.

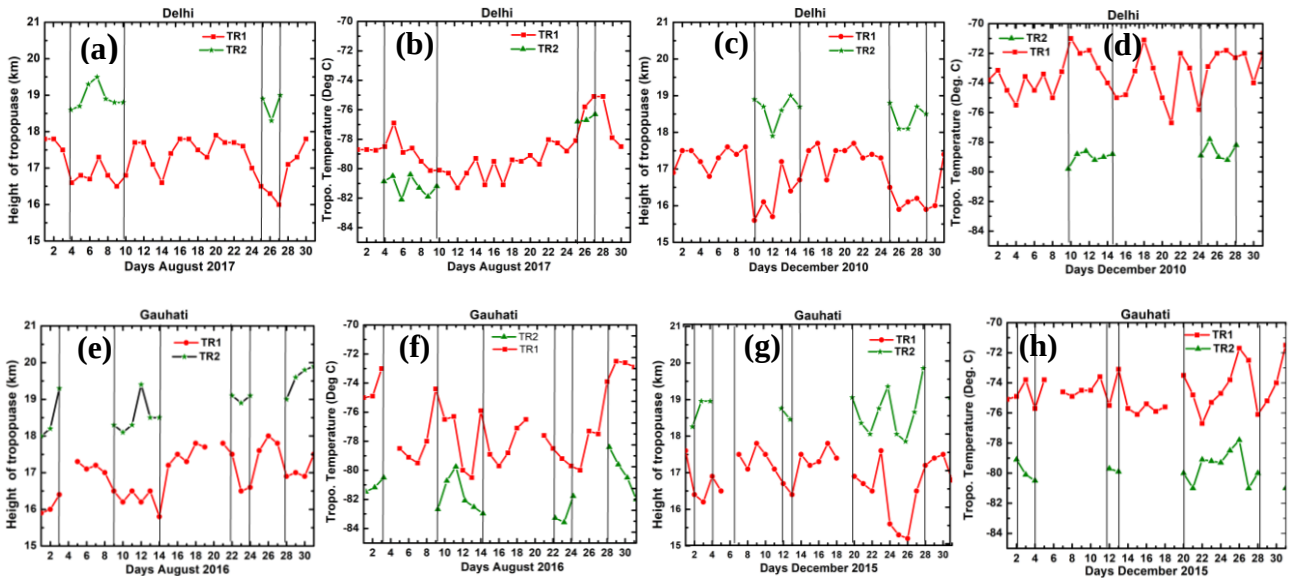

Figure S4: Daily variation of tropopause height and temperature for DT and ST days at Delhi for (a)-(b) August 2017. (c)-(d) same as (a)-(b) but for December 2010, (e)-(f) same as (a)-(b) but at Gauhati for August 2016,(g)-(h) same as (a)-(b) but at Gauhati for December 2015. DT days are separated by vertical lines and ST days are shown as TR1.

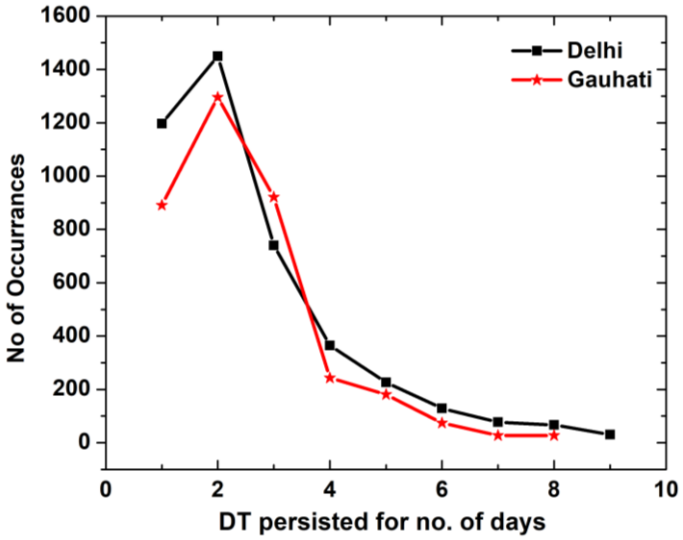

Fig. S5: Distribution indicating numbers of occurrences of DT days as a function of period of persistence over Gauhati (January 1984 – December 2017) and Delhi (January 1977 – December 2017).

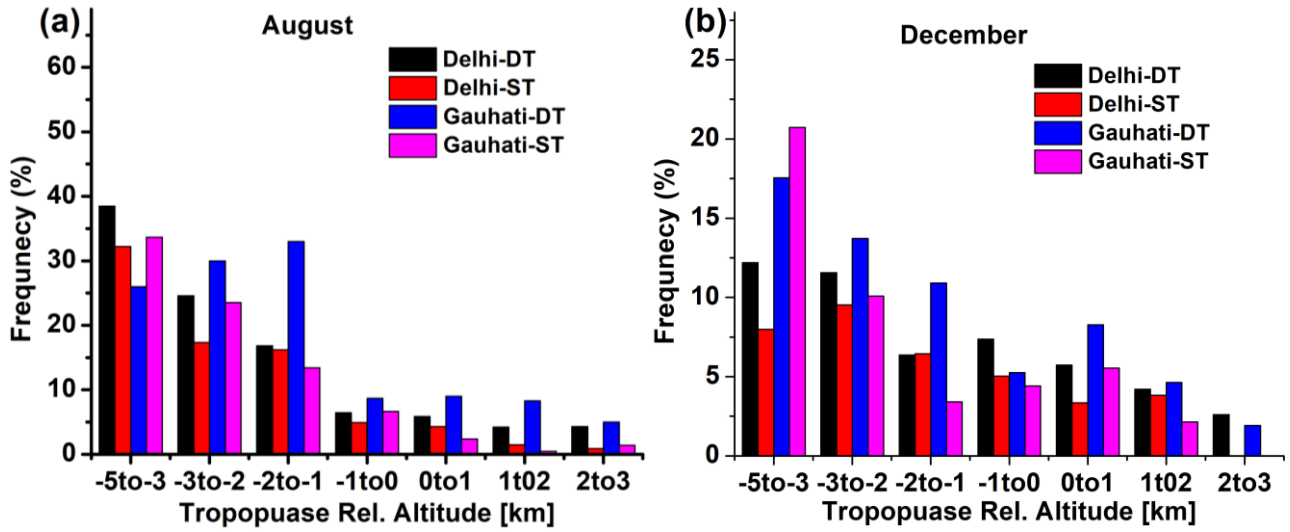

FIG. S6: Variation of frequency (%) of DT and ST days (climatology for 2003-2017) when stratified by cloud top height at tropopause-relative altitude (km) for altitude ranges of -5 to -3 km, -3 to -2 km, -2 to -1 km, -1 to 0 km, 0 to 1 km, 1 to 2 km, 2 to 3km, 3 to 5 km at Gauhati (26.14°N, 91.73° E) and Delhi (28.70°N, 77.10°E) for the months of (a) August, (b) December. In Figs (a) and (b), an altitude of 0 corresponds to the tropopause.